ABSTRACT

Title of Document: EFFECT OF COMPOSITION ON HYDROGEN PERMEATION THROUGH PALLADIUM BASED MEMBRANES

Aaron B. Leyko, Master of Science, 2013

Directed By: Professor Ashwani K. Gupta,
Department of Mechanical Engineering

Multi-component synthetic gas (syngas) mixtures produced from the gasification of coal, low-grade fuel, waste and biomass offers a novel source of hydrogen production. Gasification also eliminates much of the pollutant emissions from the combustion of these fuels. Palladium based membranes present a promising method for extracting hydrogen from syngas. Experimental results are presented from a lab scale experimental facility designed and built to examine various types of palladium and palladium alloy membranes used to harvest hydrogen from syngas. The membrane examined had a 10µm Pd layer supported on porous stainless-steel. This study used a mixture of pure gasses including hydrogen, nitrogen, and carbon dioxide to simulate syngas of different compositions. The focus aimed to determine whether composition of syngas affected hydrogen separation performance under various operating conditions. It was concluded that in addition to the hydrogen partial

pressure, the partial pressure other gas species were major controllers of membrane performance.

EFFECT OF COMPOSITION ON HYDROGEN PERMEATION THROUGH PALLADIUM BASED MEMBRANES

By

Aaron B. Leyko

Thesis submitted to the Faculty of the Graduate School of the
University of Maryland, College Park, in partial fulfillment
of the requirements for the degree of
Master of Science
2013

Advisory Committee:
Professor Ashwani K. Gupta, Chair
Dr. Michael Ohadi, Professor
Dr. Bao Yang, Associate Professor

Dedication

To mom and pop.

Acknowledgements

I would like thank my advisor, Dr. Ashwani Gupta, for providing me with the opportunity to come to the University of Maryland. Dr. Gupta's encouragement and support allowed me to grow and succeed as a researcher over these past two short years. I would like to thank Dr. Shamsuddin Ilias and his research team at North Carolina A&T State University for their assistance in providing the membranes for this study. I would also like to thank my advisory committee, Dr. Michael Ohadi and Dr. Bao Yang, for so graciously being a part of my committee.

I would like to acknowledge the members of the Combustion Laboratory at the University of Maryland: Ahmed Khalil, Vivek Shirsat, Jonathan Brooks, Hatem Selim, Henry Molintas, Islam Ahmed, Ajay Singh, Amir Eshaghi, Richard Scenna, Salisu Ibrahim, and Teresa Wierzbicki. You helped me succeed in both my academics and my research. You have also become lifelong friends.

I would like to thank my parents, Linda and Raymond Leyko, for their loving support and encouragement. I would also like to acknowledge the support of rest of my friends and family, especially Kiet Tran and Melissa Serich. Thanks for keeping me in line.

Finally, I would also like to thank the United States Coast Guard for accepting me to the Naval Engineering Postgraduate (NEPG) Program.

Table of Contents

List of Tables

List of Figures

Chapter 1: Motivation and Objectives

Billions of cubic meters of hydrogen are consumed in various industrial fields every day, and the demand for it continues to grow [1]. With increased concern over energy security, sustained supply of fossil fuels and their effect on climate change and global warming, hydrogen based energy systems are more attractive than ever before. Wider availability and utilization of hydrogen based energy can help address concerns about energy security, global climate change, and air quality. Currently, hydrogen is produced in several different ways, such as electrolysis of water, steam reforming of methane, gasification of coal and partial oxidation of oil or natural gas. These production methods are both energy intensive and expensive yet the total annual production continues to increase rapidly. One novel method of hydrogen production uses thermal conversion, such as pyrolysis and gasification to breakdown coal, biomass, wastes and low grade fuels. This reaction produces synthetic gas (syngas) comprised of primarily carbon monoxide, carbon dioxide, and hydrogen gas [2]. Nevertheless, a reliable and cost effective method of separating the hydrogen from the syngas remains elusive.

Separation by selective diffusion uses noble metal and polymer based membranes to extract the hydrogen [3]. Operating conditions as well as output preferences are key factors in determining the preferred method. Palladium and palladium alloys are ideal candidates for membrane materials, as their catalytic properties allow hydrogen to diffuse through them even at room temperature. In addition, as the hydrogen is passing through the actual metal lattice structure, these

metals are theoretically infinitely hydrogen selective. This permits levels of hydrogen purity that are not attainable by many other methods.

In this study, selective diffusion of hydrogen through palladium based membranes is examined. The effect of syngas and membrane composition are investigated under different operating conditions, such as temperature and pressure. This is a favorable separation method when the hydrogen is produced via gasification and pyrolysis. By examining membrane behavior, a greater understanding of the governing processes can be attained. With this expertise, practical solutions may be fostered for obtaining high purity hydrogen at high efficiency and low coast.

Chapter 2: Literature Review

2.1 Hydrogen Permeation

Hydrogen separation techniques can be divided into three primary categories: chemical, physical, and selective diffusion. Chemical separation consists primarily of a catalytic purification, the removal of oxygen by catalytic reaction from electrolytic hydrogen. Physical separation includes metal hydride separation, pressure swing adsorption, and cryogenic separation [3]. Selective diffusion uses noble metal and polymer based membranes [3]. The preferred method is determined through factors like feed stream, operating conditions, and desired output. The focus of this thesis is selective diffusion using palladium based membranes; as the following chapter will focus on the history, theory and current technology for that separation technique.

2.1.1 Hydrogen Permeation Process

French scientists, H. Deville and L. Troost first observed the diffusion of hydrogen through homogeneous plates of iron and platinum in 1863 [4, 5]. Most notably, Thomas Graham demonstrated the diffusion of hydrogen heated palladium and went on to work extensively with palladium foil and palladium tubes in 1866 [6]. These discoverers of palladium's ability to permeate hydrogen can be seen in figure 2-1.

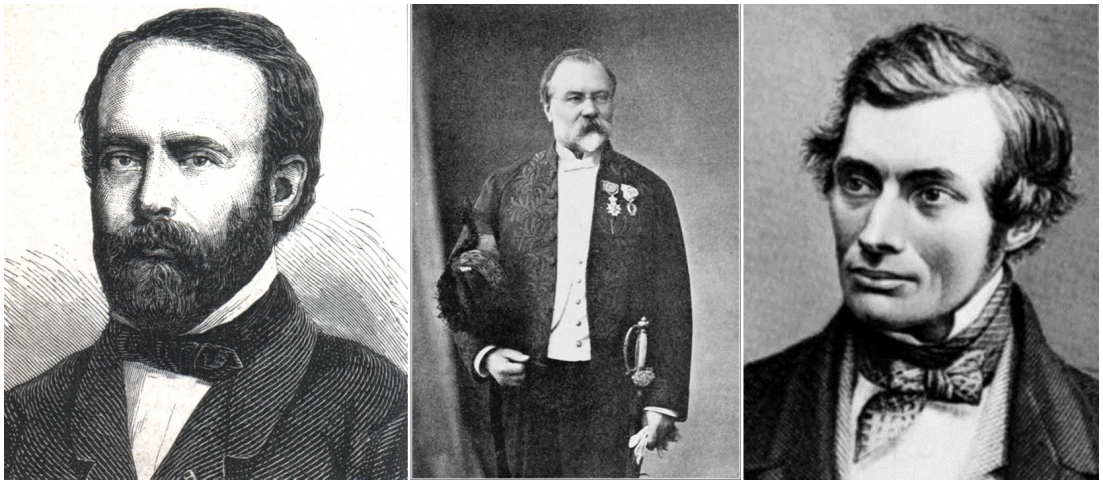

Figure 2-1 Pioneers of permeation: (Left) Henri Sainte-Claire Deville, (Center) Louis Joseph Troost, (Right) Thomas Graham [7-9].

Permeation is defined as the transfer of a gas from the high pressure side to low pressure side of a solid, non-porous material [10]. The mechanism describing hydrogen permeation through a palladium based membrane consists of seven distinct steps [11], as shown in Figure 2-2:

1) Molecular diffusion of hydrogen from the feed gas to the membrane surface
2) Dissociative adsorption on the membrane surface
3) Transition of surface adsorbed H-atoms into the metal
4) Diffusion of H-atoms through the membrane
5) Transition from the membrane to the surface on the permeate side
6) Associative desorption from the membrane surface on the permeate side
7) Molecular diffusion away from the surface into the permeate gas.

The tendency of hydrogen molecules to adsorb on the surface of palladium and dissociate is considered a non-activated process [10]. A non-activated process is

defined as a process that does not require energy to occur (no activation energy is required, i.e. an increase in temperature or heat treatment is not required). This is supported by the observation that hydrogen will permeate through palladium at room temperature and atmospheric pressure.

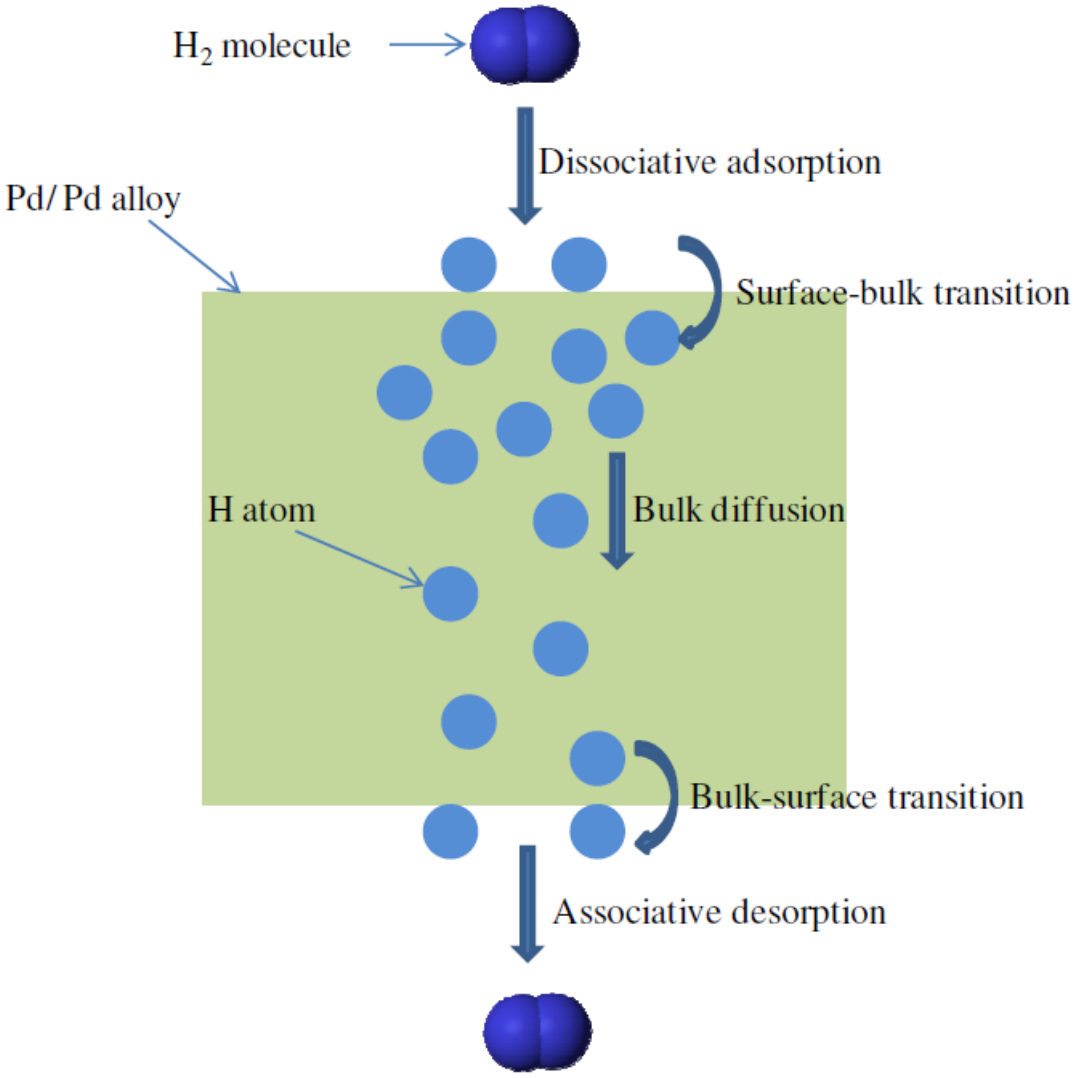

Figure 2-2 Hydrogen transport across a Palladium-alloy membrane [13].

2.2 Modeling Methods

2.2.3 Macro-scale Theory

The most common means of modeling the permeation of hydrogen through palladium membranes is to take a macro-scale approach. This high level method models the permeation process via Fick's first law, where diffusive flux is related to the concentration under the assumption of steady state. It shows how the flux goes from high concentration to low concentration and is proportional to the concentration gradient; see the equation below [14,15]:

$$J_H = -D_M \frac{\partial C_H}{\partial x} \tag{2-1}$$

where, J_H is the flux of hydrogen atoms through the membrane, D_M is the diffusion coefficient of the membrane, and C_H is the concentration of hydrogen atoms. Sievert's Law then relates the hydrogen atom concentration within the membrane to the hydrogen partial pressure, as shown in Eqn. (2-2) below [14,15].

$$C_H = K_S p_{H_2}^n \tag{2-2}$$

where, K_S is the Sieverts' Constant, and the $p_{H_2}^{\circ}$ is the partial pressure of the hydrogen molecules. The partial pressure is raised to the n^{th} power in order to illustrate the dissociation of the hydrogen molecules into hydrogen atoms at the surface of the palladium [14,15]. The hydrogen activity in solids, a_H, is defined as:

$$a_H = \left(\frac{p_{H_2}}{p_{H_2}^{\circ}}\right) \tag{2-3}$$

where, $p_{H_2}^{\circ}$ is the standard pressure of hydrogen. Expressing partial pressure in terms of activity and substituting Sieverts' relation into Fick's law, provides:

$$J_H = -D_M K_S \left(p_{H_2}^{\circ}\right)^n \frac{\partial a_H}{\partial x} \tag{2-4}$$

Integrating over the membrane thickness provides:

$$J_H = D_M K_S \left(p_{H_2}^{\circ}\right)^n \frac{a_{H,upstream} - a_{H,downstream}}{l_M} \tag{2-5}$$

If both the upstream and downstream surfaces of the membrane maintain equilibrium with their respective gas phase, then partial pressure can be substituted to give:

$$J_H = \frac{D_M K_S}{l_m} \left[p_{H_2,upstream}^n - p_{H_2,downstream}^n\right]. \tag{2-6}$$

In general, the rate of hydrogen diffusion is proportional to the difference of the n^{th} power of the upstream and downstream partial pressures. The hydrogen diffusion is also inversely proportional to the membrane thickness. The n-value is known as the pressure exponent. When n = 0.5, hydrogen atom diffusion through the membrane dominates the hydrogen transport process. However, the condition of n > 0.5 implies other processes play a role in affecting hydrogen transport. Often, an empirical 0.5 < n < 1 is used to tune the model, nevertheless, doing so masks the underlying physics.

2.2.2 Micro-Scale Theory

Micro-scale approach attempts to model each distinct stage in the permeation process and relate each effect on the other stages and the palladium-hydrogen system as a whole. In the first step, diffusion of the hydrogen from the feed gas to the surface has been modeled as the Brownian motion of hydrogen gas through a boundary layer adjacent to the membrane surface [13]. This is given by the governing equation:

$$J_H = 2\frac{D_{H_2}}{\delta}(C - C_s) \tag{2-7}$$

where J_H is the atomic hydrogen flux, D_{H_2} is the diffusion coefficient of the hydrogen gas, δ is the thickness of the boundary layer. While C and C_s are the gas phase molecular hydrogen concentration in the feed gas and at the membrane surface respectively. The diffusion coefficient will be proportional to the temperature raised to the two-thirds and inversely proportional to the pressure. The boundary layer thickness is difficult to predict as it will vary widely whether the flow is laminar or turbulent.

The surface reaction processes can be addressed as a balance between the adsorption and desorption of the hydrogen molecules on the membrane's surface. In Ward and Dao's model [11], adsorption rate, k_{abs}, of hydrogen on to the membrane surface is calculated as:

$$k_{abs} = 2Sk_{coll} \tag{2-8}$$

where S is a sticking coefficient and k_{coll} is the collision rate of hydrogen molecules on the surface. The sticking coefficient is a function of the probability of a hydrogen molecule finding two adjacent adsorption sites on the membrane's surface, given as:

$$\theta_{00} = 1 - \theta - \frac{2\theta(1-\theta)}{\left[1 - 4\theta(1-\theta)\left(1 - \exp\left(-\frac{\omega}{k_B T}\right)\right)\right]^{0.5} + 1} \tag{2-9}$$

where ω is the pairwise interaction energy, and k_B is Boltzmann's constant. Reviewing the work of Bhargav et al. the k_{abs} can be simplified to the equation:

$$k_{ads} = \left(\frac{ST^{\beta_{ads}}}{\Gamma_{Pd,surf}^2}\sqrt{\frac{RT}{2\pi W_k}}\right) \tag{2-10}$$

Where $\Gamma_{Pd,surf}$ is the volumetric concentration of interstitial sites, β_{ads} is the temperature exponent for the reaction rate of adsorption on the surface, and W_k is the

molecular weight of species k. As can be seen in equation (2-10), there seems to be a potential for a power-law temperature dependence.

Desorption on the other hand can be modeled as an Arrhenius rate constant given by:

$$k_{ads} = \left(A_{des} T^{\beta_{des}} exp\left(-\frac{E_{a,des}(\theta_k)}{RT} \right) \right) \tag{2-11}$$

where E_a is dependent on the interaction potential of surface species.

Next, the transition of hydrogen between the surface and bulk of the membrane can be modeled as [6]:

$$k_{sb} = k_{sb,\infty} exp\left(-\frac{E_{a,sb}}{RT} \right) \tag{2-12}$$

where E_a are the activation energies for adsorption, absorption, and diffusion. In Ward and Dao's work, the surface-to-bulk activation energy was found to be 13.3 kcal/mol [11].

Similar to the macro-model, the atomic diffusion flux, J_H, through the membrane bulk is concentration driven and may be modeled by the linear one-dimensional Fickian diffusion:

$$J_H = -D_H \Gamma_{Pd,bulk} \frac{X_{feed} - X_{perm}}{\Delta z} \tag{2-13}$$

Where X_{feed} and X_{perm} are the bulk hydrogen-palladium ratios adjacent to the feed and permeate surfaces, respectively and Δz is the membrane thickness. D_H is the concentration independent proportionality constant calculated from an Arrhenius-type diffusion coefficient:

$$D_H = D_0 \exp\left(-\frac{E_{diff}}{RT} \right) \tag{2-14}$$

where E_{diff} is the activation energy for hydrogen atom diffusion and D_0 is a pre-exponential factor for D_H.

The bulk metal-to-surface transition rate, k_{bs} modeled as:

$$k_{bs} = k_{bs,\infty} exp\left(-\frac{E_{a,bs}}{RT}\right) exp\left(\frac{\mu_H^E(T,X_{H,bulk})}{RT}\right) exp\left(\frac{\Delta\mu_{sol}^{\square}(T)-\Delta\mu_{sol}^{0}(T_{ref})}{RT}\right) \quad (2\text{-}15)$$

where μ_H^E accounts for the excess free energy that arises from the dissolution of hydrogen in the membrane bulk [11].

Finally, the associative desorption of hydrogen molecules are modeled as they were in the first step; however, on the permeate side of the membrane there exists a low partial pressure on hydrogen. Thus, desorption plays a dominant role. In the case of composite membranes, thin palladium based membranes (<20µm) are often supported on porous substrates. This reduces the diffusion dependence on the membrane system while providing mechanical support needed for elevated temperatures and pressures. Substrates are often considered to have a negligible effect on hydrogen permeation; however, many studies point to a non-negligible effect on permeation in composite membranes with a palladium layer below 10 µm. There is also evidence that interactions between the palladium and the porous support material at the boundary layer my affect permeation and membrane performance [13]. The resistance associated with a porous support was modeled by Bhargav et al. with the isothermal species conservation equation for a porous media [13]:

$$\frac{\partial(\emptyset_g \rho Y_k)}{\partial t} + \frac{\partial j_k}{\partial r} = 0 \quad (2\text{-}16)$$

where j_k is the mass flux of hydrogen and sweep gas through the porous media and Y_k are the species mass fractions.

2.2.3 Atomistic

Atomistic modeling to predict hydrogen diffusion using quantum chemistry and statistical mechanics with density functional theory (DFT) use first principles calculations to quantify the fundamental interactions between the membrane system components [16-34]. The models explore preferred surface phases and energetics of hydrogen diffusion into the bulk of the metal alloy. The advantage of this method is that the model theoretically captures all the physics involved in the permeation process. Currently, the complexity of a composite membrane system and present-day computational restrictions limit the usefulness of this method; nevertheless, as computer power continues to grow, atomistic modeling will play a greater role.

2.3 Permeation Membranes

Since it was discovered in the late 1800's, palladium's properties of high hydrogen diffusion, theoretically infinite hydrogen selectivity, and the ability to retain malleability have popularized this material for the production of pure hydrogen [1535,36]. Despite the obvious benefits, palladium based hydrogen separation had also been plagued with many issues including high material cost and rate-limiting minimum membrane thickness. Yet, the relative inefficiency of historic hydrogen refinement coupled with the increasing demand for high purity hydrogen have led to renewed interest in palladium based hydrogen separation.

2.2.1 Solid Palladium Membranes

Similar to other metal systems involving hydrogen, the palladium-hydrogen (Pd-H) system exhibits distinct phases depending on its temperature and composition:

the dilute α-phase, the disordered α- phase and the mixed α+β phase seen in figure 2-3 [3, 37]. The transition between these phases involves a discontinuous change in miscibility and stress on the palladium's lattice structure. In the Pd-H system, the α→ α+β transition occurs in the presence of H_2, below temperatures of 300°C. This effect is known as embrittlement. As such, minimum operating temperature above 300°C should be maintained at all times and any heating or cooling phases should be conducted in an inert environment. Nevertheless, this property allows the use of palladium naturally in gasification applications, where feed streams are typically high (300–500 °C) [2].

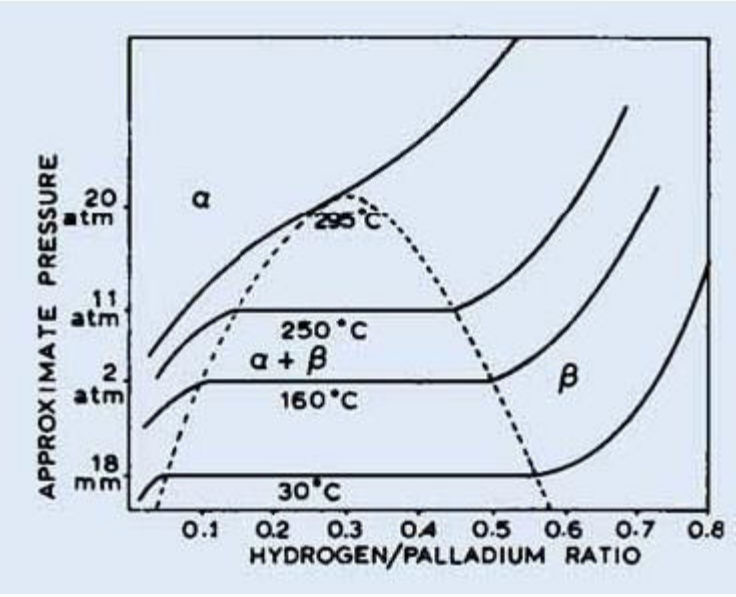

FIGURE 2-3. Correlation between hydrogen absorption in palladium versus temperature [3].

The second major challenge concerns membrane thickness. According to Fick's law, hydrogen flux is inversely proportional to the membrane thickness, while according to Sievert's law, hydrogen diffusion goes as the difference in up-stream

and down-stream hydrogen partial pressures to the half power. Thus, minimizing membrane thickness while maximizing feed-stream hydrogen partial pressure is both desired and fraught with structural problems [38,39]. Membrane poisoning was also found to be an issue in feed gases containing sulfur [36]. Embrittlement and strength issues are two primary reasons for alloying palladium with other metals such as silver, copper, gold and aluminum for hydrogen purification applications [40-45].

2.2.2 Palladium Alloy Membranes

The search for palladium alloys began when Dr. James B. Hunter discovered that using a palladium-silver alloy achieved better permeation results than pure palladium [10]. Conducted at various temperatures and pressures, his experiments concluded palladium-silver alloy composed of 20-40% silver outperformed membranes of pure palladium. The early success of Pd-Ag membranes led to considerable study of Group I-B palladium-alloys. McKinley's experiments found that high concentrations of silver in palladium can greatly expand the lattice structure in the presence of hydrogen and cause severe degradation in the membrane's structural integrity [46].

Palladium-copper alloys above 40% copper content were found to transform pure palladium's face-centered cubic (FCC) structure to body-centered cubic (BCC). The alloy's BCC β-phase was found to promote greater hydrogen transport and yielded a diffusion coefficient two orders of magnitude greater than pure palladium at room temperature [35,36]. However, this is almost equally offset by a lower hydrogen solubility that lowers the concentration gradient, limiting Pd-Cu alloys to permeation rates barely exceeding those of pure palladium [36]. Performance of several palladium alloys can be found in table 2-1, below.

Pd-alloy	Wt% of alloy metal	Average bond distance[a,b]/nm	Permeance ratio Pd-alloy/Pd
Pd	0	0.275	1.0
Pd–Y	6.6	0.281	3.5
Pd–Y	10	0.284	3.8
Pd–Ag	23	0.278	1.7
Pd–Ce	7.7	0.280	1.6
Pd–Cu	10	0.272	0.48
Pd–Au	5	0.275	1.1
Pd–Ru–In	0.5, 6	0.278	2.8
Pd–Ag–Ru	30, 2	0.279	2
Pd–Ag–Ru	19,1	0.278	2.6

[a] Bond distance of each metal: Pd (0.275), Y (0.355), Ag (0.289), Ce (0.365), Cu (0.256), Au (0.288), Ru (0.265), In (0.325).
[b] Average bond distance: $\sum_i$ bond distance of $M_i X_i$, M_i: metal, X_i: mole fraction.

Table 2-1. Hydrogen permeace of various palladium-alloys compared with pure palladium [47].

I.R. Harris, M. Norman and J.R. Thompson studied the solubility of rare earth metals. There work found cerium, yttrium, gadolinium and thorium to be soluble in palladium. These rare earth metals are roughly 30 percent larger than palladium, on an atomic basis. When alloyed with palladium, these metals acted to increase the lattice structure, surpassing that of silver, resulting in a higher hydrogen solubility gradient within the membrane and an increased hydrogen permeation rate [3,39].

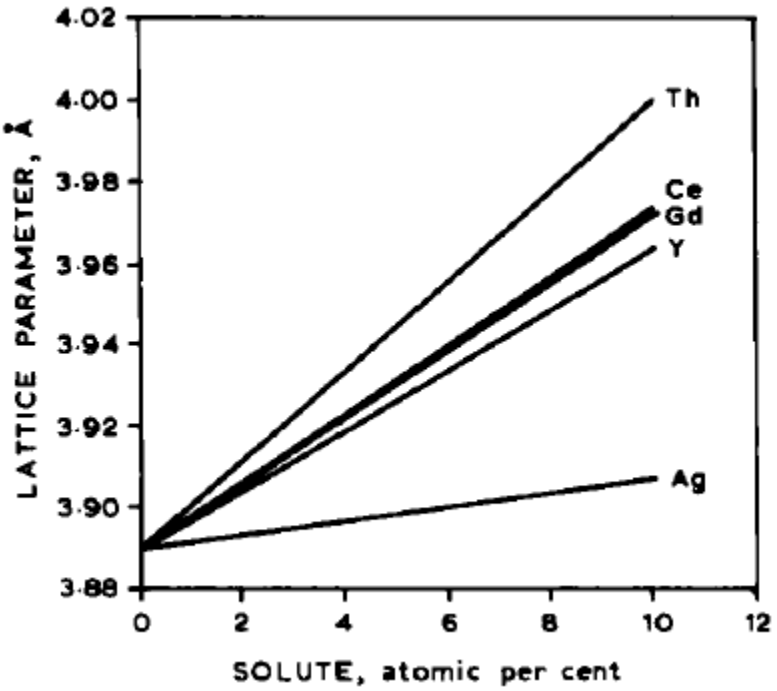

FIGURE 2-4. Rare earth metals increase the lattice spacing between atoms at room temperature significantly when alloyed with palladium compared to noble metals [39].

The difference in hydrogen solubility for the palladium-silver, palladium-cerium, and palladium-yttrium alloys creates significant differences in hydrogen concentration gradients despite similar diffusion coefficients [3].

2.2.3 Composite Palladium Membranes

Regardless of the palladium alloy composition, membrane thickness will continue to play a dominate role in the system's performance. The second factor is the inherent material cost. In an effort to reduce membrane thickness, many researchers have turned to porous supports, including Vycor glass, ceramics, or stainless steel [47]. One of the first support materials used to create composite palladium membranes was porous Vycor glass [48,49]. Vycor glass is created by

leaching the boron out of borosilicate glass (63% SiO2, 27% B2O3, 7% Na2O3, and 3.5% Al2O3) with a hot dilute acid leaving behind a network of pores from 4 to 300nm [50]. The final composition of the Vycor glass is 75–80% SiO2, 4–6% Al2O3 and 10–12% B2O3 [51]. Vycor glass boasts high temperature and thermal shock resistance, and a porosity of 28%; however, it is mechanically fragile. A summary of the properties of Pd membranes using Vycor glass supports is given in Table 2-2.

Layers on support	Method	L (μm)	T (K)	ΔP (kPa)	n	H_2 permeance 10^{-7} mol m^{-2} s^{-1} Pa^{-1}	H_2 permeability Barrer	α_{H_2/N_2}	Ref.
Pd	ELP	15	473	10	1	220	985,000	7	[86]
Pd	ELP	13	773	194	0.5	9.64	37,400	High[a]	[104]
Pd	ELP	27	673	194	0.5	4.44	35,800	High	[104]
$Pd_{94}Cu_6$	ELP	19	673	194	0.5	2.04	11,600	High	[104]
$Pd_{93}Ag_7$	ELP	22	673	194	0.5	3.57	23,000	High	[104]
Pd/glass layer with pore-filled Pd	ELP		723	100	1	0.49		520	[106]

[a] Reported as a high value in the literature.

Table 2-2. Properties of palladium or palladium-alloy membranes supported on Vycor for hydrogen separation [47].

Porous ceramic supports represent a wide-ranging category of non-metallic substrates. Several of their most notable characteristics include controllable pore size (5 – 200 nm) and the ease at which it can be shaped. One of the most common ceramic materials used in composite membrane manufacture is alumina. This ceramic is able to withstand high temperature and mechanical stresses. It is widely available in different compositions and it can be modified with the addition of intermediate layers. Ceramic supports lend themselves to tubular geometry is popular, as they are especially suited for compressive stresses. Disks shaped membranes have also been fabricated. In their simplest form, ceramic membranes have a symmetric structure with uniformly sized nano-scale pores. Though these membranes are easier to manufacture, the small pore size needed to support the palladium layer coupled with the material thickness needed to balance the feed pressure inhibit hydrogen

permeation. To address this issue, alumina supports where designed with a varied pore size, small at the Pd layer and large where mechanical support was necessary [52]. The smooth outer surface and low gas flow resistance has made the asymmetric design an optimal substrate for palladium membranes. Nevertheless, the multistep fabricating process makes this substrate comparatively costly [53]. It is important to note that care should be taken in the manufacturing of ceramic supports, as defects and roughness in the surface may yield defects or pinholes in the membrane layer [52]. Homogeneous surface characteristics, a narrow pore size distribution, and a particle size range smaller than the top layer thickness are critical to a reliable membrane. An example of using multiple thin graded layers of alumina was suggested by Oyama et al. to prevent pinholes and ensure a narrow pore size distribution while maintaining permeation rate [54]. A schematic of this can be seen in figure 2-5. Other researchers maintain that significant surface roughness of the underlying alumina support is required to anchor the membrane to the surface and prevent peeling or cracking during use [54].

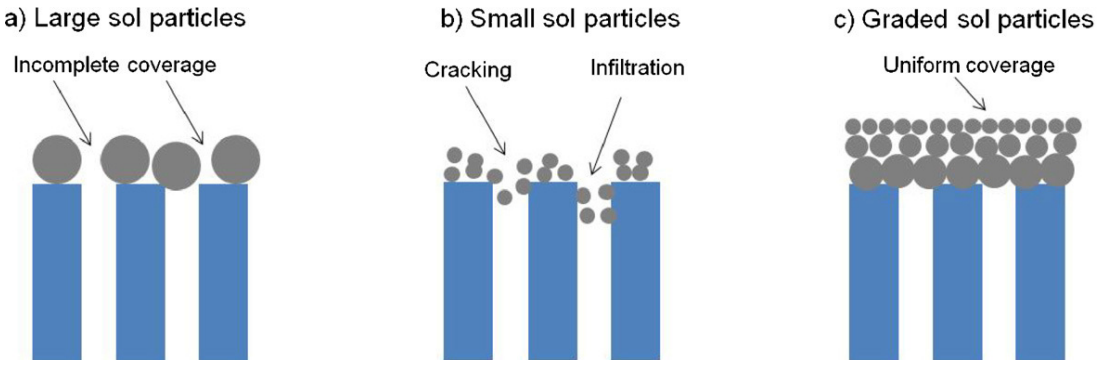

Figure 2-5. Demonstration of the effect of graded layers [47,54].

The third type substrate is the porous metal support. Porous metal has an average pore size of 0.2–100 microns, is highly shapeable, and has a thermal expansion coefficient similar to that of palladium compared to other support materials. It is also conductive, so it can be used in electroplating processes. Porous metal supports are typically formed by powder sintering or electrochemical deposition 2-3 [55,56].

Material	Linear thermal expansion coefficient (10^{-6} K^{-1})
Alumina	5.4–6.7
Borosilicate glass	3.3
Steel	11–13
Stainless steel	11–16
Palladium	11.8

Table 2-3. Thermal expansion of support materials and palladium at 293K [47].

Metallic supports are easier to seal than more fragile ceramic supports [57,58]. Among the porous metals, stainless steel is the most frequently used material due to its ease of fabrication, chemical resistance, and low cost [47]. Smallest pore size of 0.2 µm is commercially available, and it can come in disks or tubes [53]. Unfortunately, porous metal supports are more prone to rough surfaces from large pore sizes or non-uniform pore size distribution. This often causes defects or pinholes on the surface of thin palladium or palladium alloy membranes [59]. As a result, porous metal supports necessitate much thicker palladium films compared to ceramic supports. When using electroless plating, Shu et al. [59] found that a dense and defect-free palladium film under 15 µm could not be achieved on a 0.2 µm

porous stainless substrate. In another study, Mardilovich et al. [61] reported that the palladium layer needed to be approximately three times as thick as the diameter of the largest pore to obtain a He-tight membrane. By shrinking the pore size, many of the defects from the macroporous metal supports could be minimized. Several methods researchers have used to shrink the pore size include mechanically altering the surface, abrading the surface, sintering at high temperature or depositing inexpensive metals such as Ni or Cu instead of Pd [62-65].

Currently, there are several methods for attaching the membrane to the porous structure. Layers of palladium and palladium alloys have been attached via chemical vapor deposition, electroless plating, electroplating deposition, and physical vapor deposition.

First reported by research teams Kikuchi et al. and Uemiya et al, electroless plating (ELP) this is presently the most common technique for preparing palladium membranes [66-68]. ELP plates metallic films on a substrate by the reduction of metal complex ions in solution without the application of an external electric field, see figure 2-6.

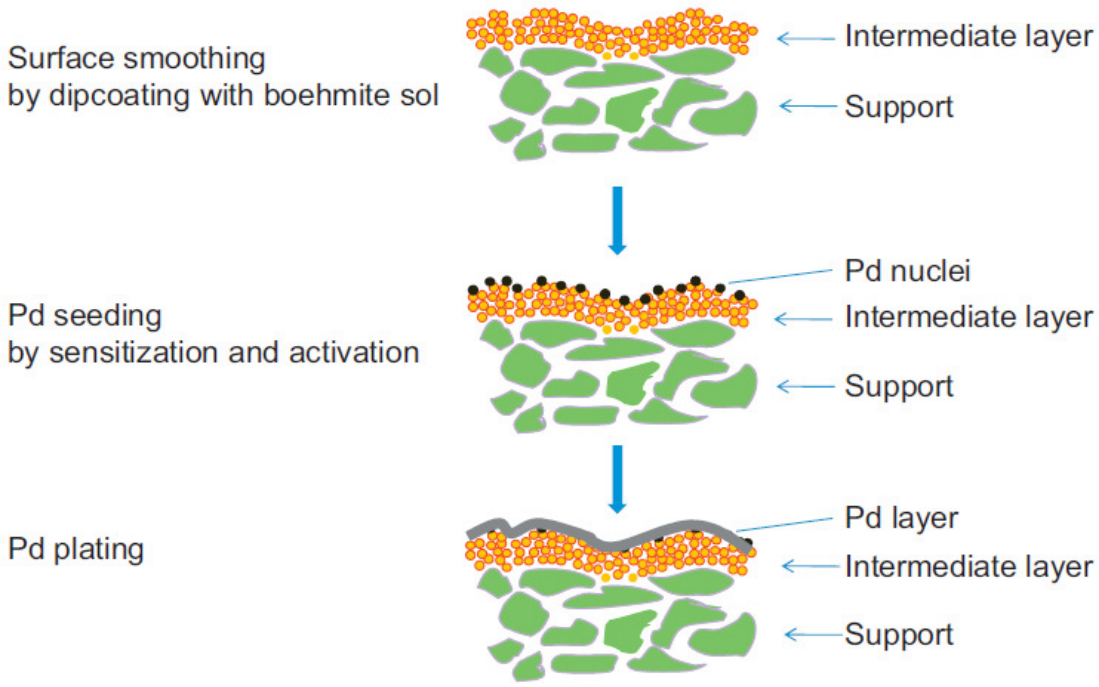

Figure 2-6. Conventional electroless plating procedure [47].

The reduction of metallic salt complexes on the surface of the support material requires activation step to initiate the reaction. This is because the plated metal on the surface acts as the catalyst for further reaction [69]. As a result, the support surface must be seeded with palladium precursor particles. This is accomplished by sensitization and activation. Sensitization is usually accomplished by dipping the smoothed support into acidic tin ($SnCl_2$ or $SnCl_4$) solutions. Once that is complete, the process of plating of the palladium layer on the activated surface may begin. With this method, rough surfaces can be smoothed via deposition of intermediate layers.

The advantages of ELP include ease of coating on shaped materials, minimal cost, and simple equipment [70]. However, the activation and sensitization pre-treatment steps make the ELP process complicated and time-consuming. One

challenge of ELP is the formation of Pd alloys in the presence of an unequal reduction potential of the metallic ions. As observed for the case of Pd–Ag, the resulting uneven deposition caused dendritic growth of the membrane layer [71]. Samhun Yun et al, reported that an adjustment in metal/hydrazine concentrations would narrow the gap between metallic ions reduction potential and solve this issue [45].

Chemical vapor deposition (CVD) uses thermal decomposition of volatile precursors to deposit thin films of palladium on the surface of a porous support. CVD is most often used when a precise palladium layer thickness is required [69]. In one study, $PdCl_2$ was used by Ye et al. to manufacture a composite palladium membrane on an α-$Al2O_3$ disk [72]. In addition, a schematic of a forced-flow CVD facility used by Itoh et al. to create tubular composite palladium membranes of only 2-4 µm thick may be seen in figure 2-7 [73].

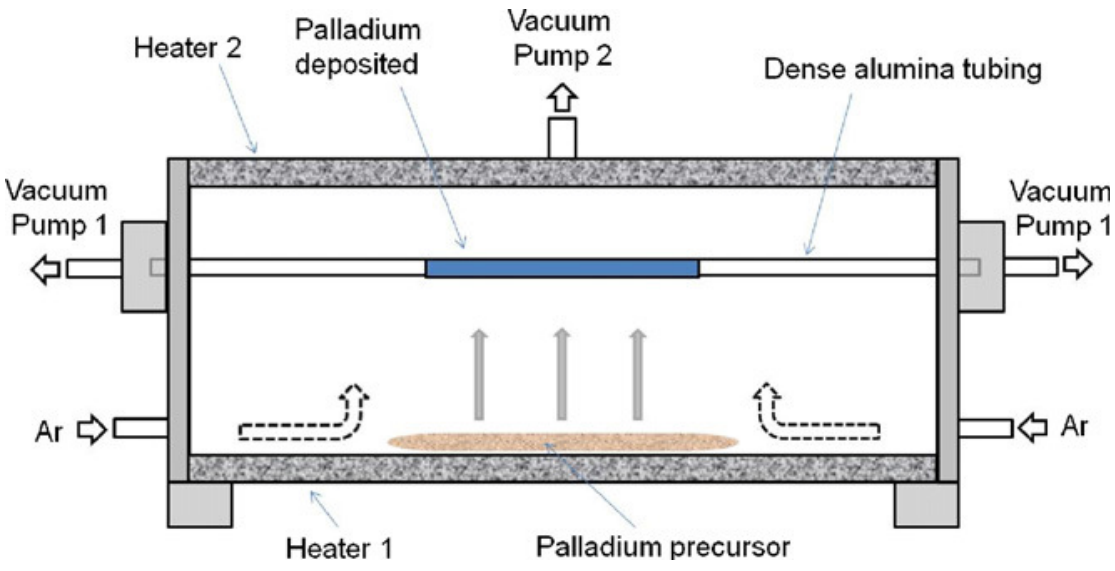

Figure 2-7. Apparatus for preparing tubular Pd composite membranes by means of forced-flow chemical vapor deposition [47,73].

The advantages of CVD include better quality control, and palladium layers of thicknesses less than two micrometers. On the other hand, CVD's costly constituents, high-vacuum, process conditions, and possibility of residual carbon contamination limit the general use of this technique [72,74,75]. It is also interesting to note that membranes manufactured by CVD have palladium so thin that diffusion is no longer rate limiting. In fact, surface effects, hydrogen dissociation, and resistance due to the porous support play a dominant role [13,69,75].

Physical vapor deposition (PVD) works by bombarding a solid precursor with the aid of a high energy source such as a beam of electrons or ions in a vacuum [76]. Material is jettisoned off the precursor's surface, landing on the surface of the porous support. One example of PVD, Sputtering deposition, uses excited Ar ions to dislodge individual palladium atoms from a target. The palladium atoms diffuse to the substrate, where they deposit on the surface, as seen in figure 2-8 [77].

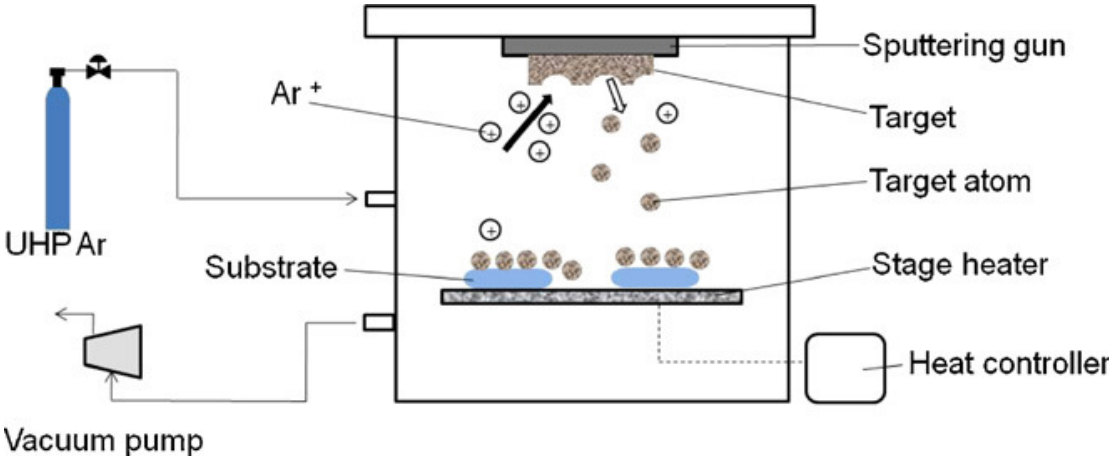

Figure 2-8. Schematic diagram of magnetron sputtering deposition apparatus adapted from [47,77].

PVD allows better control of the film composition, phase and thickness than electroless plating; however, high vacuum and power requirements make the equipment quite expensive [78]. In addition, PVD can only be used on flat substrates.

Electroplating deposition (EPD) employs electrical current to reduce dissolved metal cations. The electric potential transports the cations through the liquid-phase electrochemical and deposits them on a substrate acting as a cathode [79,80]. A diagram can be seen in figure 2-9.

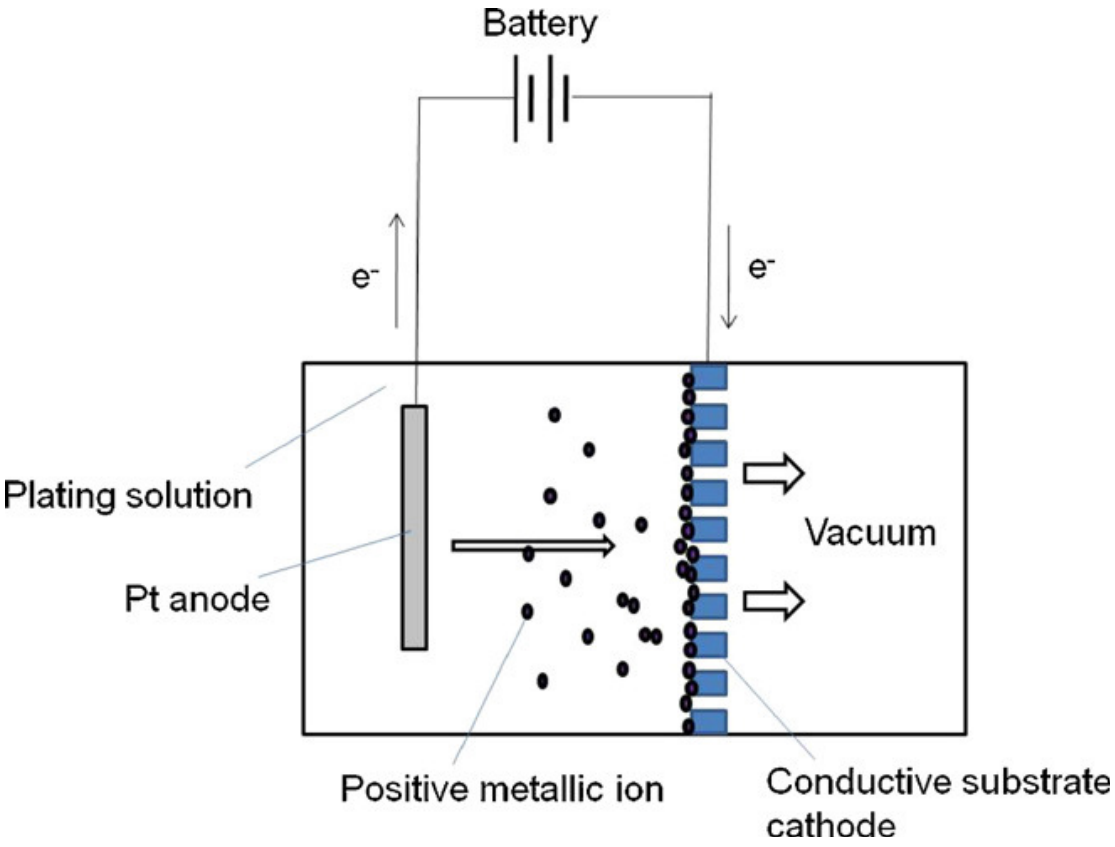

Figure 2-9. Schematic diagram of vacuum electrodeposition system [47,81]

EPD uses simple, cost effective equipment. Film thickness can also be controlled by varying electroplating time and current density [81]. Nevertheless, this method can only be used to generate coherent metal coatings.

2.4 Prior Experimentation

2.4.1 Hydrogen Separation Facilities

Arguably the most important piece of a hydrogen separation facility, besides the membrane, is the membrane housing. The membrane housing must be able to withstand extreme temperature and pressure. It must also endure possibly corrosive feed gas. All this must be accomplished with maintaining a secure barrier between the feed and permeate gases. In addition, the geometry of the housing can also be designed to maximize the desired interaction between the membrane and both feed and permeate gases.

Finally, the experimental setup must use components chosen for the specific pressure, gas sources, flow controllers, a temperature level, and anticipated permeate stream. Gauges must also be put in place to measure the necessary and desired parameters. The following is a brief review of the membrane housings and experimental facilities that guided the design of the housing used in this study.

Designed over a half century ago, Makrides et al. membrane housing laid down the foundation for many future housing designs, including the one in this study [38]. The casing in which they tested their membranes can be viewed schematically below in Figure 2-10. This housing incarcerated all the basic functionality of current membranes. The membrane was secured to the end of the stainless steel tube using electron beam welding [38]. Makrides et al. pressurized the system with a pump on the permeate side or by the presence of a high pressure gas on the feed side, while pressure was regulated via the valve (24) on the bottom of the diagram [38]. In case

of cold feed steam temperature, electric heating elements (26) maintained an elevated housing temperature [38].

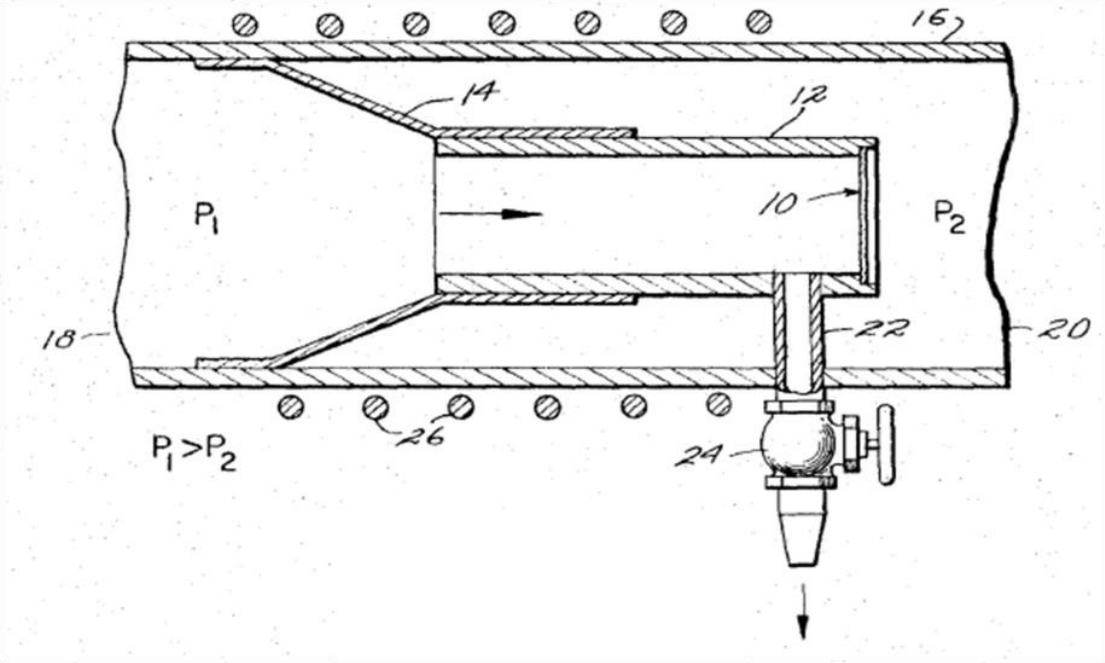

Figure 2-10. This schematic of the membrane housing used by Makrides et al. The Group V-B metal membrane (10); The feed gas inlet (18); permeate outlet (20); system pressure regulation and non-permeated gas outlet (24); Heating elements (26) [38].

Later, sweep gas was added to alleviate the need for a vacuum pump on the permeate side or extremely high pressures on the feed side. Sweep gas prevented the hydrogen build-up on the permeate side of the membrane, effectively increasing partial pressure difference without increasing the total system pressure [12,82]. As the hydrogen pressure gradient drives permeation, hydrogen build-up on the permeate side would decrease the permeation rate. This is especially important for thin membranes lacking mechanical support. Commonly used as sweep gases for experimentation include, nitrogen and argon. However steam would be a practical

choice for industrial use due to the ease of separation from hydrogen through condensation.

As mentioned before, it is pivotal to attain a leak-free diffusion around the membrane. Palladium based membranes are greatly useful due to their nearly infinite hydrogen selectivity and ability to produce ultra-pure hydrogen, the presence of leaks and errant feed stream gasses undermine these benefits. Dissimilar thermal expansion coefficients in the membrane and housing materials may lead to leaks at operating conditions that were not present at room temperature and atmospheric pressure. Careful consideration must therefore be taken to ensure all seals are designed with final operation conditions in mind. Early in their studies, Ilias et al. found that their stainless-steel housing suffered from leakage at high temperatures [83]. Through the use of graphite and copper seals, they produced a casing that would self-seal at high temperatures. A schematic of Ilias et al.'s design can be seen in Figure 2-11 [83]. The outer shell of the casing in Figure 2-11 was made of stainless steel (AISI 310) whereas the inner parts were made of titanium. The graphite seals were used against the ceramic edges of their membrane while the copper seals were placed between the stainless steel tubes [83]. Ilias et al. reported that there was no external detection of hydrogen in experiments conducted with the updated assembly [83].

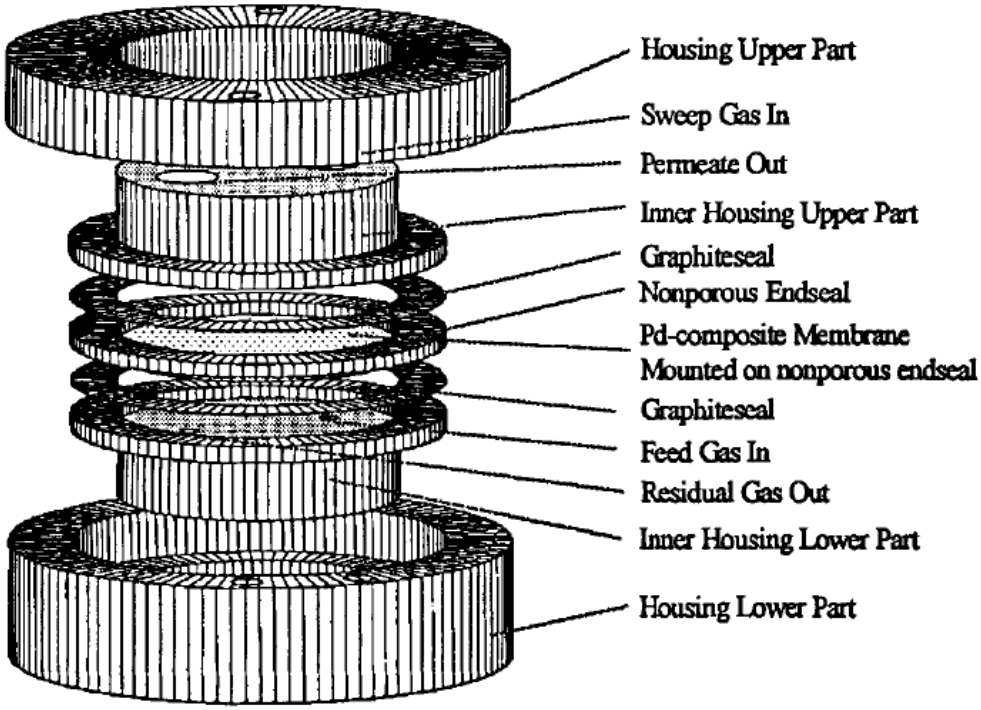

Figure 2-11. Schematic of a self-sealing (at high temperatures) membrane housing. This cell was designed by the Velterop Ceramic Membrane Company of the Netherlands, Model LTC Type K-500 [83].

A membrane casing assembly used by Howard et al. was held together using novel TIG welding and brazing techniques developed by the U.S. Department of Energy's (DOE) National Energy Technology Laboratory [82]. These methods were necessary to ensure no damage to the membrane due to extreme heat normally associated with welding operations [82].

Once the membrane is secured in an adequate housing, the rest of the experimental system must be put in place. The housing designed by Ilias et al. was incorporated into the experimental facility seen in Figure 2-12 [83]. Ilias et al. mounted the membrane housing in a tubular furnace and used stainless steel tubes for their gas lines with the [83]. Feed gas and sweep gasses are shown in yellow and red

respectively. Mass flow rates for the gas streams were collected by flowmeters at the feed and sweep inlet and rotameters at the outlet. System pressure was monitored with pressure gauges and maintained with valves and a pressure transducer. Using a syringe, Ilias et al. took samples from the sample ports indicated by green arrows. A Gas Chromatograph (GC) was then used to analyze sample [83]. The use of multiple sample ports is allows gas composition to be tested at different stages of the permeation process. An improvement on this facility would be the addition of a direct connection of the sampling ports to the GC. Installed sampling lines would increase make data gathering easier and less labor intensive. The facility depicted below represents a relatively common setup for hydrogen permeation experiments, and it influenced the design of the facility employed in this study.

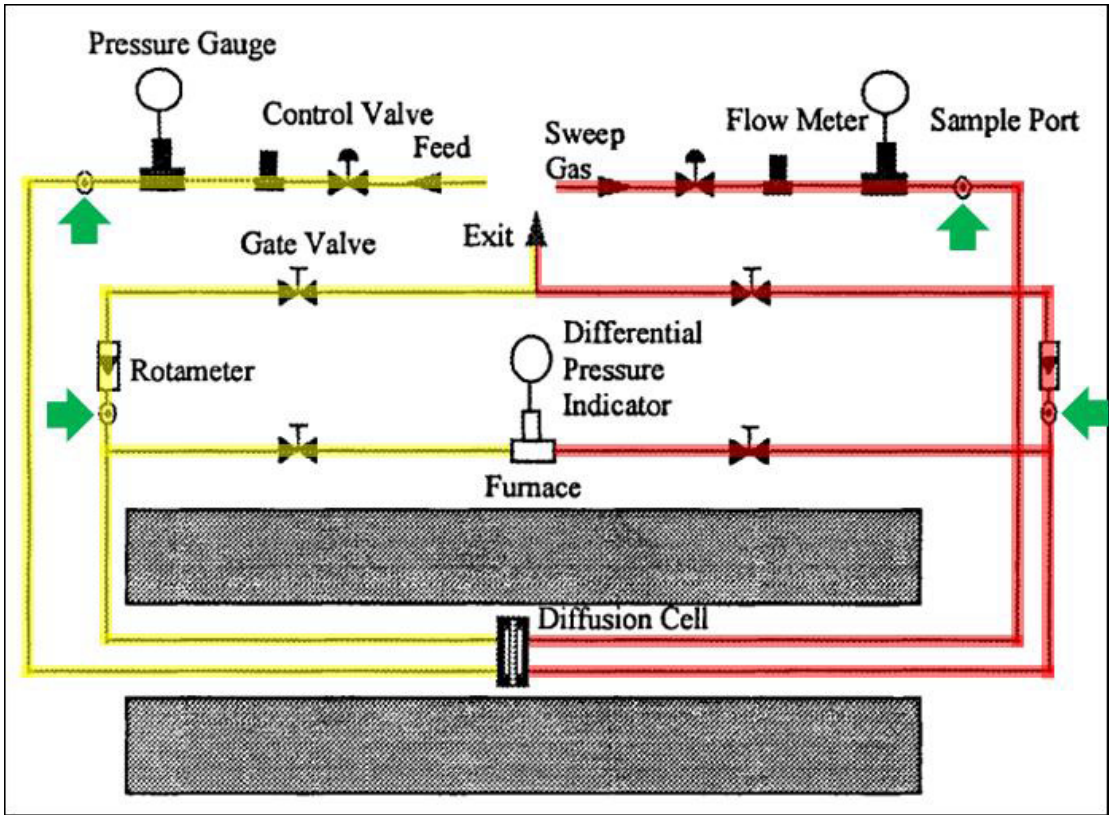

Figure 2-12. Experimental facility for hydrogen separation [83]. The yellow lines highlight the feed side, the red lines highlight the sweep side and the green arrows indicate sample ports.

The facility depicted by Figure 2-13, however, is much more sophisticated. Gielens et al.'s facility was designed to study membrane use in the production of hydrogen through methane steam reforming [84]. Their setup was optimized to study the effects of carbon dioxide and steam on hydrogen flux through palladium and palladium-silver membranes. Their goal was to determine if the presence of the two gasses would impede the dissociation of hydrogen at the surface [84]. Figure 2-13 shows water was added to the feed gas and heated to form steam, then cooled again after passing over the membrane.

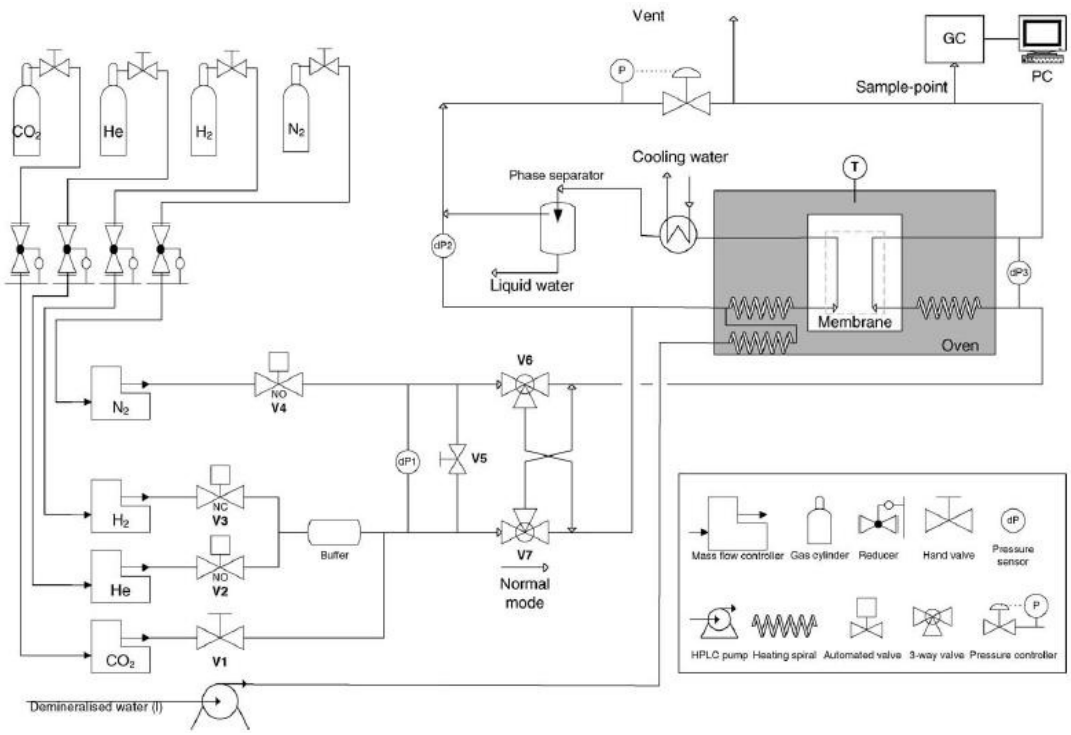

FIGURE 2-13. Experimental facility for the study of the effects of CO2 and steam on the hydrogen separation process [84].

The similar design concepts can be found throughout literature. The two facilities shown in Figures 2-12 and 2-13 have many similarities; nevertheless, each is uniquely suited to accomplish the different objectives of each research team. Identifying the experimental goals and objectives beforehand is the most important element of constructing an effective facility. As experimental goals tend to change over time, a design that is modular and easily adaptable can be of great advantage. Likewise, In addition to meeting the minimum experimental requirements, an emphasis should be placed on ergonomics. A researcher will likely spend many hours working on an experimental facility. Convenient access to displays, knobs, and dials as well as automatic data collection, transfer, processing, and back up will almost always prove to be design time well spent. Finally, researchers should take pride in

their facilities design and construction. A quality facility will usually produce quality results.

2.5 Gassification and Syngas

As mentioned before, leveraging renewable energy sources are critical to breaking the dependence on the world's dwindling fossil fuel reserves. Until then, current fossil fuel energy conversion practices must be made environmental benign. A solution to help solve both of the issues lies in gasification. Gasification holds a key to realty reduce the polluting byproducts of fossil fuel use. Gasification also allows clean conversion of municipal, industrial, and agricultural wastes, including plastics and rubber, biomass and other low grade fuels into energy. The end-product of gasification, hydrogen containing synthetic gas or syngas, was most importantly in this study.

2.5.1 Synthetic Gas Production

Gasification uses a gasifying agent to heat carbonaceous material without combustion, producing gaseous fuel, or syngas. The heating value of the gases produced is generally low to medium. The desired chemical composition of the syngas determines gasifying agent used. A second important process that occurs during fuel conversion is pyrolysis. This consists of the thermochemical decomposition of the fuel due to the elevated temperatures alone, without the gasifying agent, yielding gas, and tar and char residues. Pyrolysis reactions have relatively low activation energy as compared to gasification reactions [37]. As such, the organic material is initially pyrolized. Next, the secondary products are gasified

leaving the final syngas and ash [85]. The work by Gomaa et al. reported Steam was found to be the desired gasifying agent to achieve high hydrogen yield. In addition, the final composition of the syngas is a function of the gasification temperature, steam to carbon ratio and pressure [37]. Carbon, carbon monoxide, carbon dioxide, hydrogen, water (or steam), and methane reactions play the most significant role in the gasification of solid carbon [85]. These include:

Combustion reactions:

$$C+½O2 \rightarrow CO,\ \Delta H = -111\ MJ/kmol \quad (2\text{-}17)$$

$$CO+½O2 \rightarrow CO2,\ \Delta H = -283\ MJ/kmol \quad (2\text{-}18)$$

$$H2+½O2 \rightarrow H2O,\ \Delta H = -242\ MJ/kmol \quad (2\text{-}19)$$

The Boudouard reaction:

$$C+CO2 \leftrightarrow 2CO\ \Delta H = +172\ MJ/kmol \quad (2\text{-}20)$$

The water gas reaction:

$$C+H2O \leftrightarrow CO+H2,\ \Delta H = +131\ MJ/kmol \quad (2\text{-}21)$$

The methanation reaction:

$$C+2H2 \leftrightarrow CH4\ \Delta H = -75\ MJ/kmol \quad (2\text{-}22)$$

Reactions from 2-20, 2-21 and 2-22 are the most important reactions in the char-gasification step and both are endothermic reactions. These reactions are reduced to the following two homogeneous gas reactions.

Water-gas shift reaction:

$$CO + H2O \leftrightarrow CO2 + H2,\ \Delta H = -41MJ / kmol \quad (2\text{-}23)$$

The steam methane reforming reaction:

$$CH4 + H2O \leftrightarrow CO2 + 3H2\ ,\ \Delta H = +206MJ / kmol \quad (2\text{-}24)$$

Figure 2-14 shows a simplified reaction sequence for the gasification of carbonaceous matters.

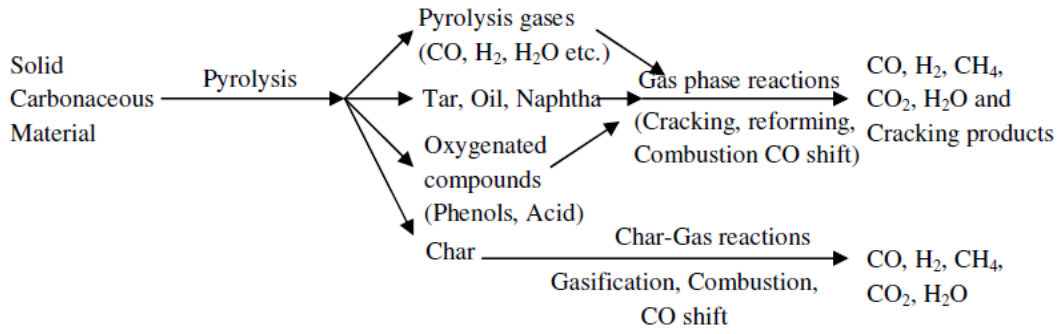

Figure 2-14. Reaction sequence for gasification [13]

2.5.2 Syngas Composition

As seen in figure 2-14, the final product of gasification and the composition of syngas consist primarily of N_2, CO, CO_2, CH_4, H_2O and most importantly H_2. The CO, CH_4, and H_2 can be pumped directly into a reactor and converted into energy. However, the syngas may also be further processed in the case of this study H_2 may be removed. Once removed, high purity hydrogen is necessary for the operation of fuel cells; furthermore, the absence of H_2 in the syngas aids in using the reverse water gas shift reaction to maximize methane and CO production. As for the other gasses in the feed stream, they may affect the hydrogen purification process. It is no coincidence that several studies have been conducted to determine the effect of these gases on hydrogen permeation. Understanding how feed stream impurities influence both hydrogen permeation and membrane longevity could lead to improved membranes dependability and permeation methods. This challenge was a major motivation for different investigations including this study.

A study conducted by Wang et al. used a composite membrane of thin palladium layer mounted on corundum (α-Al_2O_3). They subjected the membrane to feed streams of N_2, H_2, and an H_2-N_2 (1:1 molar ratio) [86]. Pure hydrogen was desired; thus, no sweep gas was used in the experiments. Initial experiments on a newly prepared membrane were conducted with the use of pure gas feed streams. The membranes were exposed to H_2, N_2, and H_2, sequentially, for varying time periods. During the first pure hydrogen phase, flux increased over time then steadied out. Immediately following the pure hydrogen phase, the membrane underwent a pure nitrogen phase, in which permeation dropped to zero. Finally, in the third phase, the nitrogen was cut off and hydrogen restarted. When this occurred, permeation again increased to the original steady state values of the first phase; however, it took significantly longer. Wang and colleagues concluded that there was no membrane deterioration as a result of hydrogen exposure during the first phase and that the more gradual increase in permeance in the third phase was a result of the clearing of impurities from the active sites [86]. Wang et al. repeated the experiment with a fresh membrane, substituting argon for nitrogen. The results showed a much smaller effect on the time to reach a steady state permeation rate. A further experiment was conducted with the H_2-N_2 mixture (1:1 molar ratio). Wang et al. found that experiments conducted below 550°C would experience a gradual drop in permeation, calling this effect "deactivation." They also found that the effects of deactivation could be revered at operating temperatures above 550°C. Wang et al. attributed deactivation to the competition for active sites by NH_x compounds that may have formed on the membrane surface [86].

Other studies found carbon monoxide to affect hydrogen flux even more than nitrogen [87]. Nevertheless, several studies of H_2-N_2 and H_2-CO mixtures concluded that the negative effects of both nitrogen and carbon monoxide decreased with increasing temperature [87]. Like nitrogen, it was theorized that carbon monoxide

molecules may be competing with hydrogen molecules active sites and reducing hydrogen flux; however, confirmation of this hypothesis remains elusive [87].

A study by Guazzone et al. found that steam initially has a negative effect on hydrogen permeation. Gradually, hydrogen flux increased beyond that of the initial pure hydrogen feed stream at temperatures in the 350-450°C range [88]. They reasoned that this is a result of the membrane scavenging additional hydrogen molecules produced in the reverse water gas shift reaction [88]. This result may prove valuable with the effective use of syngas to increase both the pure hydrogen and gaseous fuel. Steam was also believed to free the membrane surface of impurities Hydrogen flux was also found to increase following steam operations. This is believed to be a result of the steam cleansing the membrane of surface of impurities such as CO and CO_2 [88].

Hydrogen permeation varies greatly with the composition of the feed gas. In addition, the effect of feed gas composition on permeation is a function of exposure time, temperature and both total and partial pressures. The chemical properties of the palladium or palladium alloy membrane also affect reactions with feed stream impurities. Steam was shown to have a positive effect on permeation, while carbon monoxide, carbon dioxide and nitrogen seem to reduce permeation. Argon was found to be neutral.

Chapter 3: Experimental Setup

3.1 Membrane

3.1.1 Membrane Characteristics

All experiments in this study were conducted using composite palladium and palladium alloy membranes mounted on porous stainless steel disks. These membranes were graciously prepared by Dr. Shamsuddin Ilias, a Research Professor in the Department of Mechanical and Chemical Engineering at North Carolina A&T State University (NC A&T) and the members of his research team. Palladium foil was mounted on the stainless steel supports then annealed. The membrane covered the entire surface of one side of the stainless steel disk. The palladium and palladium alloy membrane layers mounted on the porous support was reported to have a thickness of 10 microns. The disks measured one inch in diameter, with thickness of 0.0625 inches. The stainless steel disks were reported to have a 0.2 micron pore size. Figure 3-1 below shows two membranes prior to experimentation. The membrane on the left was used in this study. In agreement with literature, members of Dr. Ilias's team specified that the palladium membranes should not be operated below 300 degrees Celsius as there was a risk of hydrogen embrittlement [3,12,36,89]. Dr. Ilias's team also recommended an operating membranes temperature of 350 degrees Celsius. It is important to note that the research team at NC A&T did not have experience running hydrogen separation experiments above 600 degrees Celsius or 30 psig [90].

Figure 3-1. Photograph of palladium (left) and palladium-copper (right) membrane.

3.1.2 Membrane Stress

As composite membranes are used for their enhanced strength, a stress calculation was conducted to determine the maximum force supportable by a thin membrane on porous stainless steel. Van Rijn et al.'s equation for estimating maximum pressure on a thin ductile membrane was first examined [91]:

$$P_{max} = 6.4 \frac{X_m \sigma_{yield}^{\frac{3}{2}}}{l E_y^{\frac{1}{2}}} \tag{3-1}$$

where, X_m is the membrane thickness, σ_{yield} is the yield stress, l is the length of membrane's shortest side and E_y is Young's modulus [92]. It is well known that the yield stress and Young's modulus are temperature dependent. As such, Eq. (3-1) makes predictions of the maximum pressure based on material selection, thickness,

and operating temperature. While the palladium layers were only 10 to 12 microns, this thickness relative to the diameter of the 0.2 micron pore size of the stainless steel support invalidated the thin membrane assumption [90]. As a result, a traditional shear stress calculation and yield strength comparison was made to estimate maximum pressure. Assuming a feed pressure of 1000 psi is used, which is much higher than any pressure used experimentally in this setup, the following calculations have been completed to determine if the palladium could withstand the pressure in unsupported areas (i.e. where there are pores in the stainless steel). The shear stress, τ, is found by dividing the force, F, by the shear area, A_s, as in Eqn. (3-2) below.

$$\tau = \frac{F}{A_s} \tag{3-2}$$

and

$$A_s = \Delta z(\pi d_p) \tag{3-3}$$

Where shear area is the thickness of the membrane, Δz, multiplied by the perimeter of the pore. The force was calculated by dividing the pressure, P, by the area over which it was acting or the area of the pore, given by:

$$F = P * A_p \tag{3-4}$$

and

$$A_p = \pi\left(\frac{d_p}{2}\right)^2 \tag{3-5}$$

Substituting in equations 3-2, 3-3, and 3-4 into 3-5, a model for estimating max operating pressure is attained:

$$P_{max} = \frac{4\tau_{max}\Delta z}{d_p} \tag{3-6}$$

The reported range for the yield strength of Pd is between 35 and 205 MPa, or 5,076 and 29,733 psi [92,93]. Taking the lowest yield strength and plugging it into equation 3-6, the maximum pressure sustainable by the palladium membrane supported on the porous stainless steel support was estimated at 7000 MPa or 1,015,264 psi. This estimate puts the max membrane pressure well above the 100 psi hydrogen separation facility design pressure. Even considering a pore size of 100 microns, maximum pressure would be 14 MPa or 2,030 psi, well above the operating pressures of this study

3.2 Membrane Housing

This study utilized the membrane housing designed and built by James et al. A brief description of the design proses follows below.

The membrane housing was designed to create a seal around the membrane while also withstand high temperatures and pressures. The housing was made of Type 303 stainless steel and consisted of two major components, an upstream side and a downstream side. While in operation, the two sides were flanged together with the membrane sandwiched in between. Upstream and downstream sides possessed a gas inlet and outlet to allow for the circulation of feed and sweep gasses, respectively [90]. Despite the basic similarities between the two sides, the internal geometry varied significantly. The flange style housing permitted easy membrane swopping while maintaining a pressure seal during use. The membrane was gasketed by copper washers on both the feed-side and permeate-side. To ensure an adequate pressure seal, the copper washers were prepared by sanding with light machine oil in conjunction with both 600 and 1000 grit sand paper [90]. The washers were then boiled in water for five

minutes to remove any oil residue that could provide surface contamination. The copper washers had a one inch outer diameter with a 5/8 inch inner diameter, leaving 0.3068 square inches of surface area exposed for hydrogen permeation [90]. The feed stream inlet had a 1/4 inch diameter opening, 1/8 inch away from the membrane surface. The opening directed the feed gas directly at the center of the membrane, which would then flow radially out from the center, over the membrane surface and exit the housing from an outlet port, as shown in Figure 3-2.

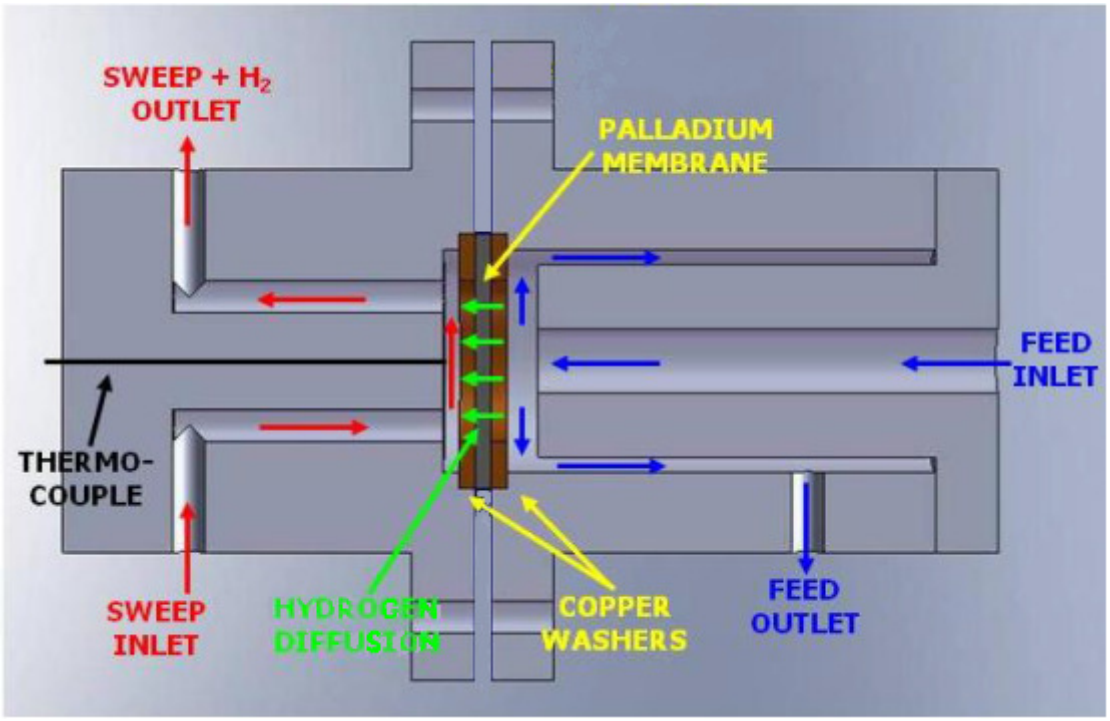

FIGURE 3-2. Schematic cross-section of Pd Membrane Housing [90].

The feed side of the housing was designed by James et al. to maximize the feed chamber surface area and feed stream gas exposure to the membrane [90]. As flow increases over the membrane the effective partial pressure would drop as a result of the inverse relationship between volumetric flow velocity and pressure or Venturi

affect. It was desired to maximize the flow rate in order to assume a constant partial pressure of the component gases despite the permeation of hydrogen. On the other hand, it was also desired to keep the flow rates as low as possible for minimum loss of local pressure at the membrane due to Venturi effect. As such, the membrane-feed exposure volume was 0.0384 cubic inches and with a surface area to volume ratio of eight. During the permeation experiments, measurements were taken at the lower and upper limit of the facility's operational capabilities. No difference in hydrogen permeation was detected, thus one flow rate was chosen and held constant though out all experimentation. Further effects of the feed side flow rate over the membrane were not investigated in this study but have been recommended for future work. The sweep chamber on the permeate side had a smaller volume with the sweep gas bisecting the membrane surface as it passed across. The permeate side of the housing also contained the local thermocouple. This was placed in the housing and as close to the membrane as possible to give and accurate membrane temperature reading. Thus, the temperature data acquired from this thermocouple was assumed to be the system temperature. A more detailed description of the membrane housing design process can be viewed in reference [90].

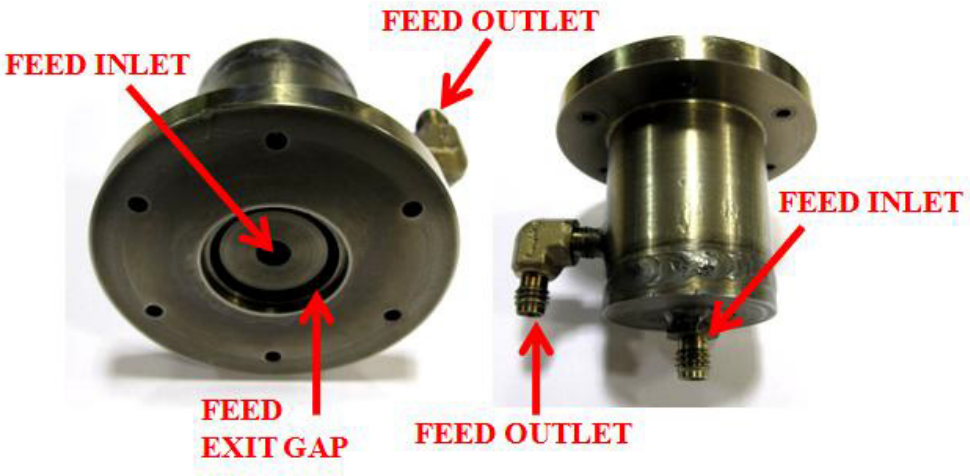

FIGURE 3-3. Membrane housing feed side components [90].

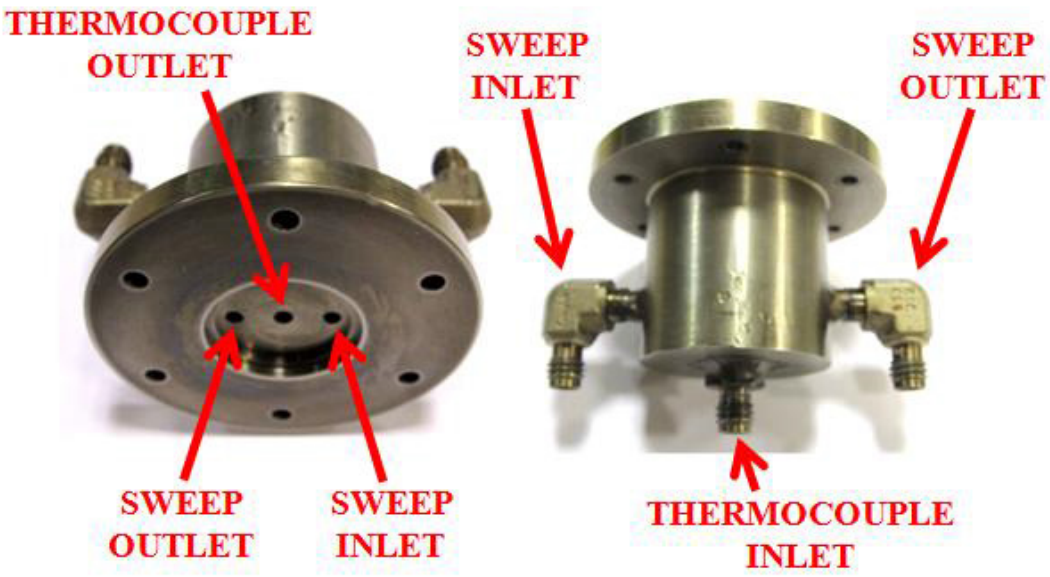

FIGURE 3-4. Membrane housing sweep side components [90].

Upon assembly, the screws of the flanged sides were tightened in a star-pattern using up to 20 in-lb of torque to minimize leaks. All connections to the housing were made via Swagelok® fittings. Figure 3-5 below shows the casing completely assembled

with washers, membrane in place [90]. The casing as displayed is ready for use in the hydrogen separation facility.

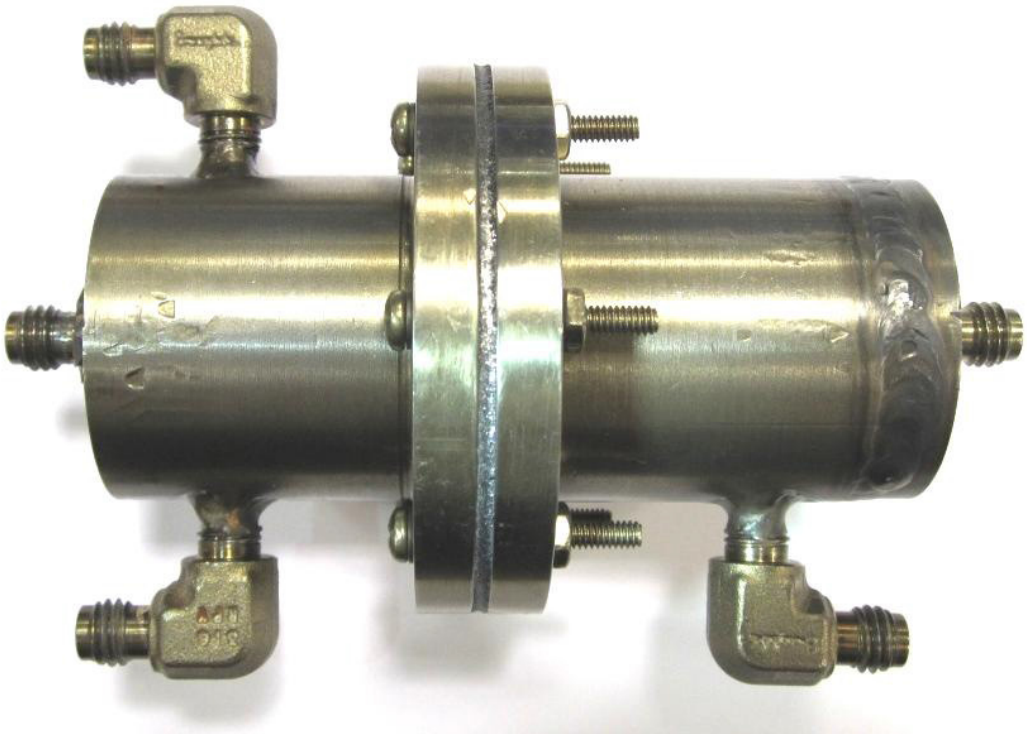

FIGURE 3-5. Assembled membrane casing.

3.3 Hydrogen Separation Facility Design

While the original membrane housing from James et al. was used in this study, the recommendations from the previous work allowed for an updated separation facility. The updated facility retained its feed and sweep gas capability while incorporating an increased feed mixture capability which allowed for ternary feed gas experimentation. The sweep gas was designed with a cross-connect valve to allow for an inert environment during heating and cooling operations. The feed stream upon exiting the membrane housing was designed with a connection to be either vented or routed to the GC for analysis. The gas mixture leaving the permeate side of the membrane

housing was primarily connected to the Gas Chromatograph for analysis. After leaving the gas bottle and regulator, each component gas entered the facility via an AALBORG GFC-17 gravimetric flow controller. GFC-17 gravimetric flow controller incorporated a proportionating solenoid valve and a closed loop control circuit to continuously compare the mass flow output with the desired flow rate. Automatic valve adjustments maintained the desired flow parameters. The GFC monitored the gas flow by shunting a small portion of the flow from the main flow passage to a sensor tube. Within the sensor tube, heat flux was introduced in two locations. Gas flow carried the heat from the upstream coil to the downstream coil windings, resulting in a temperature dependent resistance differential that was detected electronically. The onboard control system calculated the instantaneous rate of flow comparing it to the linearly proportional gradient in the sensor windings. The GFC's had a flow range of 2.5-100% and an accuracy of ±1.5% of full scale. Feed system pressure was maintained by a pressure gauge and pin valve immediately downstream of the membrane housing feed-stream outlet. The pressure gauge was an Omega Engineering Inc. model DPG-1000B with accuracy down to ±0.25%. A flowmeter was placed immediately after the permeate outlet for the same reason. During various experiments, additional pressure gauges were added at key points throughout the system to monitor the pressure. A schematic diagram of the facility can be seen in Figure 3-6 below.

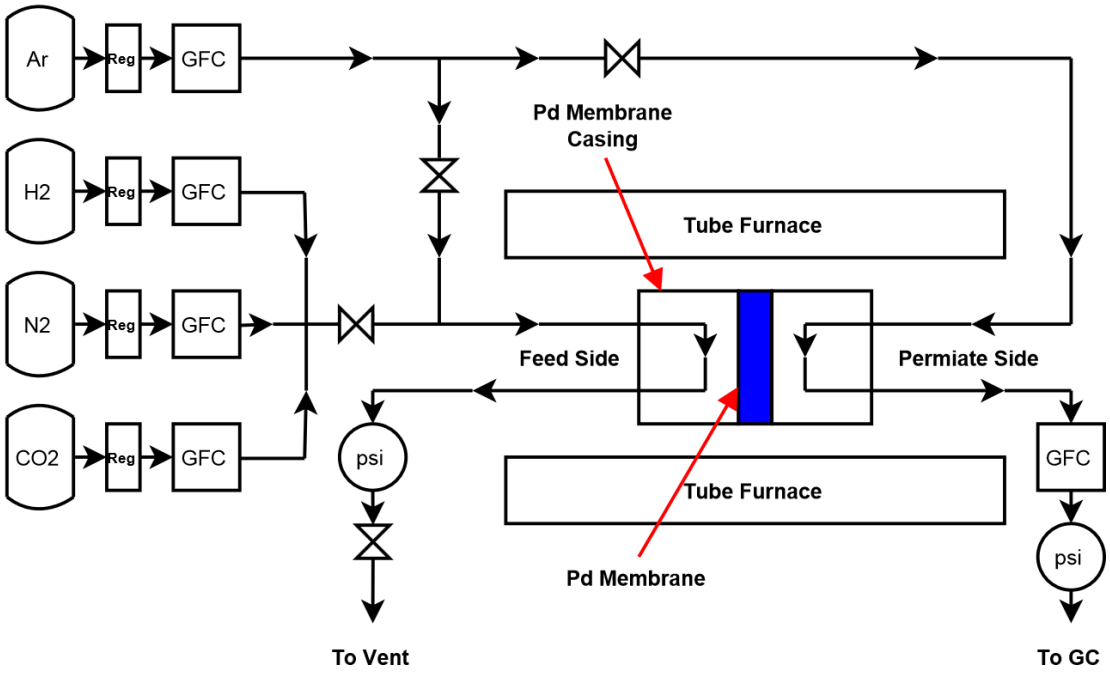

Figure 3-6. Schematic diagram of the hydrogen separation facility.

The furnace used was a Carbolite Model HST 12/--/300/301 Single Zone Hinged Tube Furnace. The furnace had a 1200°C temperature range with a heated length of 11.75 inches and an inner tube diameter of four inches.

When placed inside the tubular furnace, the membrane housing rested on two 1/8” steel rods. All gas lines are attached via Swagelok® fittings as shown in Figure 3-7 below.

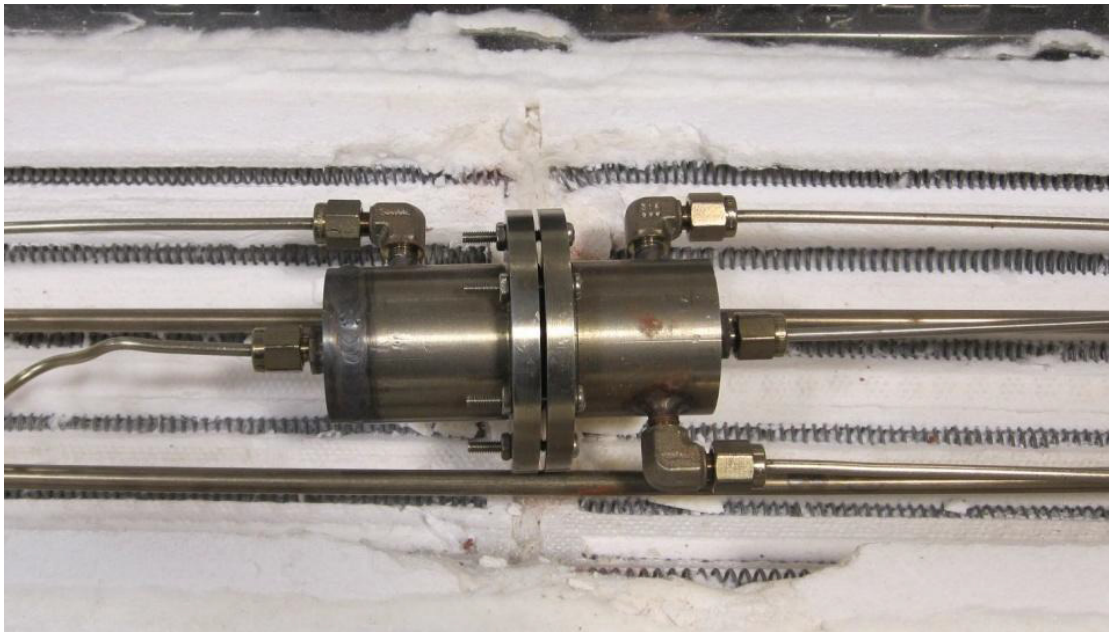

Figure 3-7. Membrane housing mounted inside Carbolite furnace.

The thermocouple was fitted on the sweep side of the housing and secured also via the Swagelok® to prevent leakage. The thermocouple was of the K type, produced by Omega Engineering Inc. and had an accuracy of ±1.0% over the experimental range. The gas chromatograph used for these experiments was an Agilent 3000A Micro Gas Chromatograph (μGC), seen in figure 3-8.

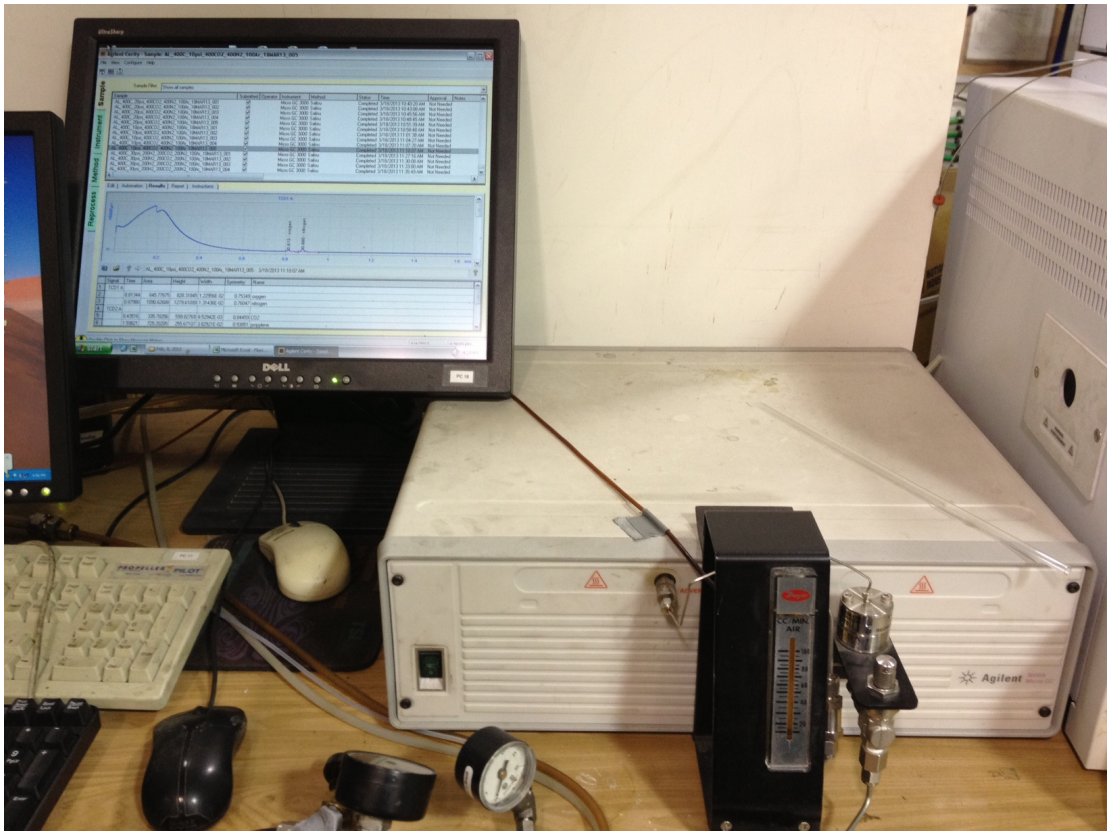

Figure 3-8. Agilent 3000A Micro Gas Chromatograph used in experiments.

The GC system includes a heated injector, sample column, reference column, thermal conductivity detector (TCD), electronic pressure control (EPC) hardware, gas flow solenoids, and control system. The permeate analysis process within the GC occurred in three basic steps: injection, separation, detection. During the injection phase, the sample enters the micro GC's heated manifold. The manifold regulated the samples' temperature while directing it into the injector [94]. The injector then propelled the sample into to the column, while a vacuum pump helped draw the sample through the other end. Next, the sample entered the separation column, where it was separated into its component gases. Gas chromatography works on the principle that molecules of varying size and mass will travel at differing rates with the carrier gas through separation column substrate. These differences allow for component separation and

eventual detection and identification based on travel time. Choice and thickness of column coating, column length and diameter, choice of carrier gas and flow rate, and oven temperature play an important role in successful data gathering.

After leaving the separation column, the sample gas flows through the thermal conductivity detector. The sample gases enter the detector, passing over hot filaments. The varying thermal conductivity of the sample molecules caused a change in the electrical resistance of the sample filaments when compared to carrier gas reference filaments [94]. Several pressure tests were conducted on the facility during construction to ensure effectiveness. Recommendations for future system modifications will be discussed in chapter 5. An image of the original facility can be seen in figure 3-9, while the updated final facility can be seen in figure 3-10, below.

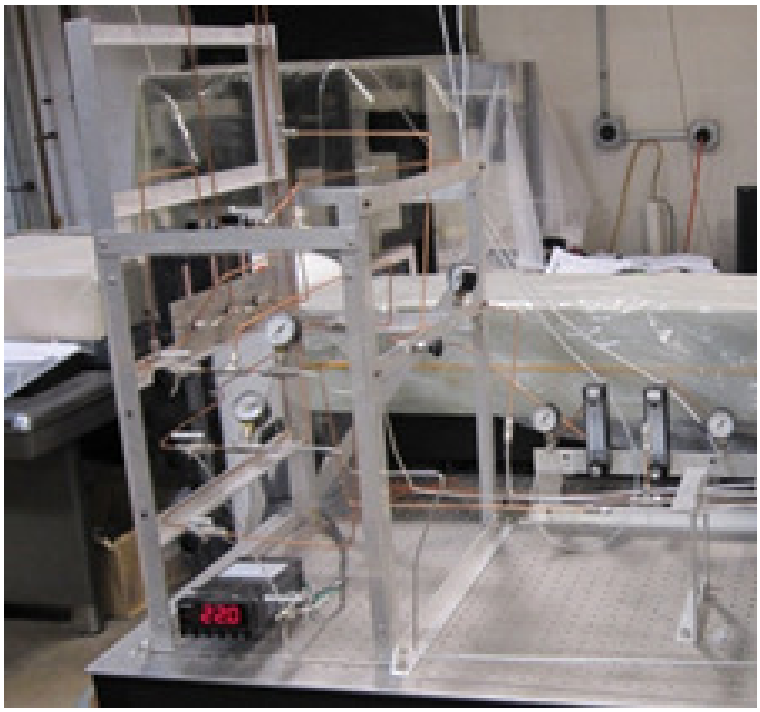

Figure 3-9. Legacy hydrogen separation facility.

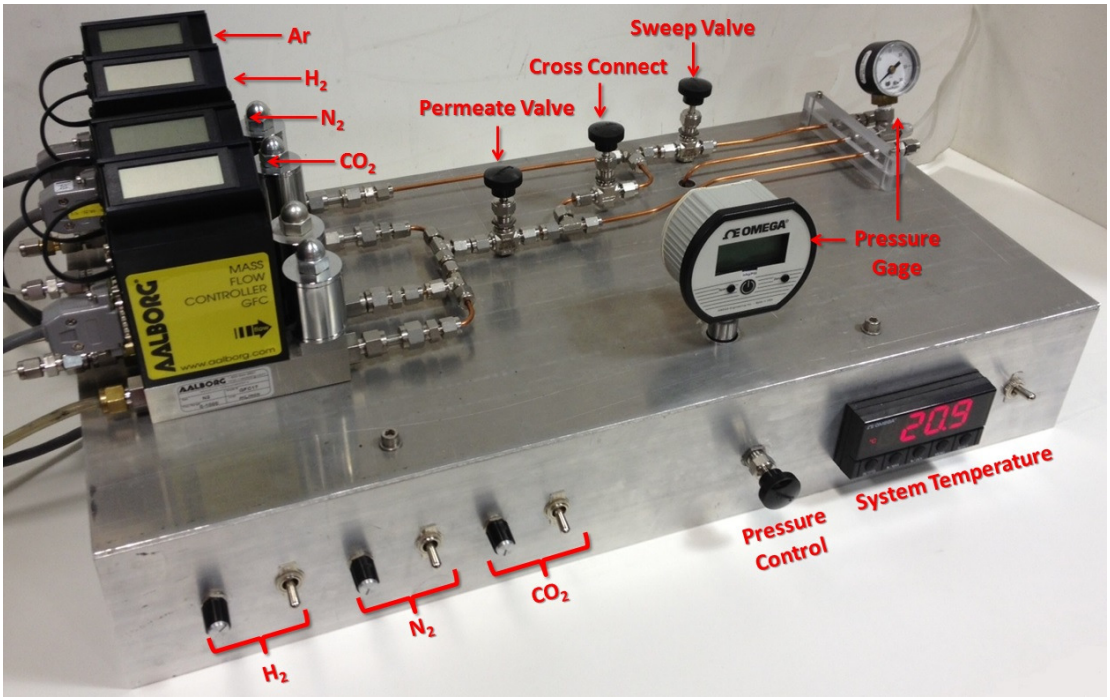

Figure 3-10. Updated hydrogen separation facility.

3.4 Uncertainty Analysis

3.4.1 Measurement Chain

To extract actual values from the measured values, the measurement chain relation was used.

$$M_{corr} = M_{undist} - \Sigma E + \Sigma C \pm \delta C \pm \delta M_{obs} \quad (3\text{-}7)$$

Where M_{corr} is the corrected value, M_{undist} the measured value, ΣE the error associated with the measurement, ΣC and δC the correction terms for the error and linked uncertainties, respectively, and δM_{obs} the uncertainty related to the measurement. The error and correction terms were neglected and the uncertainty analysis was primarily focused on the δM_{obs} value. Therefore, Eqn. (3-1) was simplified to Eqn. (3-2).

$$M_{corr} = M_{undist} \pm \delta M_{obs} \tag{3-8}$$

The overall uncertainty of the measurement was found by applying the root sum square (RSS) method.

$$e_r = \sqrt{\sum \left(\frac{\partial f}{\partial x_n} e_n\right)^2} \tag{3-9}$$

Using RSS allowed for the derivation of the expression to be used for the δM_{obs} term in Eqn. (4-2).

3.4.2 Sources of Uncertainty

Anytime a measurement is taken there will always be uncertainty associated with the measured value. The primary sources of error for the experiments conducted in this study were the pressure gauges, the thermocouple, mass flow controllers, and the gas chromatographer (GC). The values for the uncertainty of the pressure and temperature measurements were assumed to be the given error for the specific instrument. In the case of the pressure gauges, the reported accuracy was ±2% mid-scale [95]. The thermocouple error was reported to be the greater of ±2.2°C or ±0.75% [96]. Due to the temperature ranges used in the experiments, the latter error was used for the thermocouple readings. The accuracy reported for the gas flow controllers was ±1.5% [96].

No error or accuracy values were reported in the GC manual; thus, three to five measurements were taken at each sample location during all experiments. The standard deviation for the three values was then used to find a 95% confidence interval. The confidence interval was then assumed to be the error associated with the GC for each measurement. The uncertainty associated with any leakage was

calculated using RSS analysis. For example, hydrogen leak in a binary H_2-CO_2 mixture was calculated by comparing feed stream gas composition to permeate stream gas composition acquired using the GC. That data was then plugged into the relation:

$$H_L = \frac{[CO_2]_p[H_2]_f}{[CO_2]_f[H_2]_p} \tag{3-10}$$

Applying Egn. (4-3) to Eqn. (4-4) yields the RSS relation for uncertainty associated with hydrogen leak in a binary H_2-CO_2 mixture.

$$\delta M_{obs} = \left[\left(\frac{[CO_2]_p}{[CO_2]_f[H_2]_p} e_{H_2,f}\right)^2 + \left(\frac{[H_2]_f}{[CO_2]_f[H_2]_p} e_{CO_2,p}\right)^2 + \left(\frac{[CO_2]_p[H_2]_f}{[CO_2]_f^2[H_2]_p} e_{CO_2,f}\right)^2 + \left(\frac{[CO_2]_p[H_2]_f}{[CO_2]_f[H_2]_p^2} e_{H_2,p}\right)^2\right] \tag{3-11}$$

where the e_n values equal the values of the 95% confidence interval for each measurement. Results of the uncertainty analysis are displayed as error bars in the following chapter.

Chapter 4: Experimental Results and Analysis

4.1 Pressure Testing

The work in this study has stood on the shoulders of prior work concerning hydrogen separation. Before any experimentation could begin, the dormant hydrogen separation facility needed to be closely examined and brought back into operational condition. The first order of business was to ensure all measurement equipment was functioning properly and within calibration. Pressure gauges were known to be within calibration yet they were tested to double check against any malfunction. The thermocouple mounted in the membrane housing was new and arrived precalibrated. The Gas Chromatograph was calibrated following the instructions in the operational manual. The process consisted of a "bake out" phase and a calibration phase. The Bake out phase was an automated process whereby the GC ran up the internal temperature while flowing pure span gas through the separation columns. This procedure was meant to clean any impurities out of the column that remained from any previous experiments. The bake-out process took a couple days to complete. Next the GC was calibrated using a bottle of calibration gas. The calibration gas consisted of the gasses that were likely to be studied in very precise ratios. The GC then analyzed the calibration gas and the readings for each gas were corrected if necessary against the bottle's known composition ratio.

Once all the measurement equipment was determined to be in good working order, all the hardware, joints, and fixtures of the facility were inspected for material

condition and connection. Finally leak tests were conducted, as in James et al.'s work, to confirm the operation of the facility.

4.1.1 Pressure Testing Membranes

First the housing assembly with membrane emplace was tested at twice the operating pressure. These tests were conducted at ambient and operational temperatures for several hours. Membrane pressure tests were carried out on both the membrane housing in its entirety as well as by just pressurizing the permeate side of the membrane. All pressure tests were conducted with the noble gas, argon. Argon was chosen because from literature it was found that in tests with argon resulted in no deviation in membrane performance [90]. This was important because of the finite supply of membranes and the long lead-time for replacement. Extra care had to be taken to ensure as much data as possible is extracted from every specimen. In addition to the inert effects of argon, palladium and palladium alloys are only permeable by hydrogen. Thus, as long as the palladium layer was intact, a feed stream pressure test conducted with argon should yield no pressure drop. This would provide an accurate indication of membrane surface integrity. A sample of test results can be seen in figure 4-1.

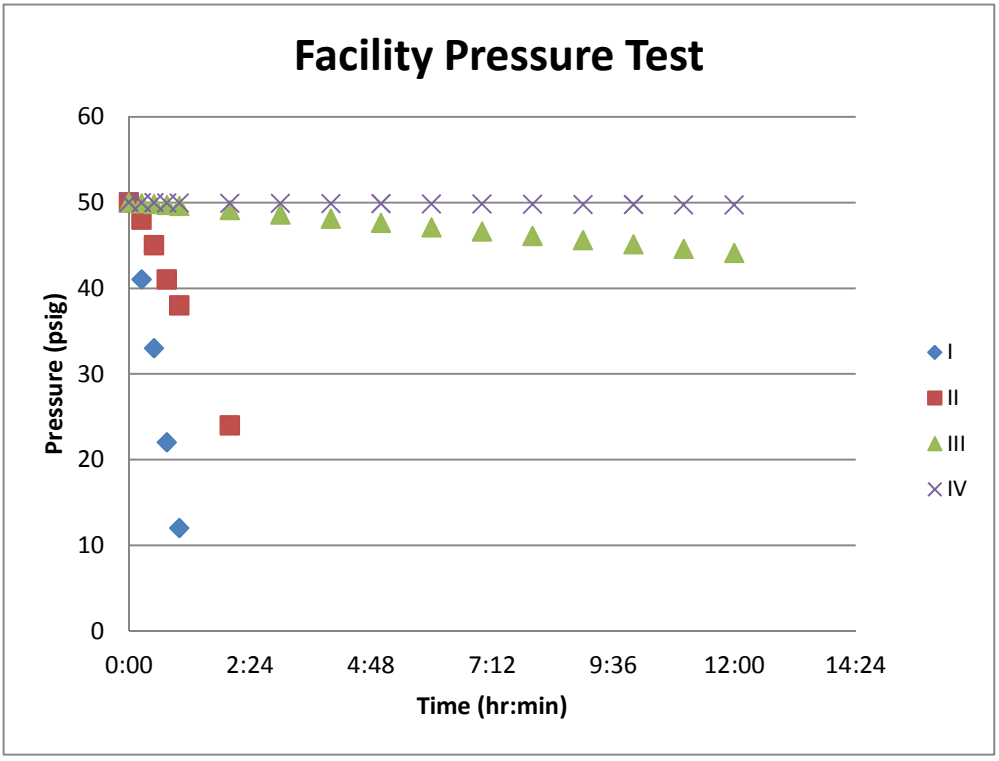

Figure 4-1. Hydrogen separation facility pressure testing results. Tests 1 and 2 were conducted at ambient temperature while test 3 and 4 was conducted at 300 degrees Celsius.

The first set of tests was conducted with a goal to determine if the palladium layer was intact. Tests one through three were completed at ambient temperature. The outcome of test one was disheartening. The facility would not hold pressure. It was evident that a rapid leak was present. A technique of applying a solution of soapy water to the joins of the system quickly reviled loos Swagelok fitting. This was tightened and confidence was restored. The second and third tests went much better; however, a gradual loss in pressure indicated an additional slow slight leak in the system. Previous work recommended that the experiments were to be conducted above 300 degrees Celsius [90]. Thus, pressure test at the higher operational temperatures would not only be more applicable but also, more successful due to thermal expansion of the housing possibly creating an improved seal. With negligible

pressure loss over 12 hours, test three shows a vast improvement over the first two tests and the next stage of testing could begin. The same testing was repeated; however, the second time around the permeate side was pressurized. This was important to ensure no leaks were present on either side of the membrane. This test was also conducted at temperatures 300 Celsius. The results of this test showed even more improvement over the 12 hour period and can be seen in figure 4-1 as test four. The slight pressure loss in test three versus test four was thought to have indicated the possibility of a slight leak in the palladium layer of the membrane. This theory would be confirmed later during permeation testing.

4.1.2 Pressure Testing Facility

The last pressure test was conducted on the entire facility at 300 Celsius. This test would give a final confirmation of the hydrogen separation facility's operational status. The first couple of tests indicated leaks but these were quickly discovered via soapy water and remedied. Once all the fittings were tightened, the facility had no trouble holding pressure for the twelve our test period.

4.2 Permeation Experiments

4.2.1 Hydrogen Permeation Experiments

Once the pressure testing was completed, it was finally time to prepare for the permeation tests. The ultimate goal of this study was to determine the effects of syngas composition on hydrogen permeation. Before that could be accomplished a test plan needed to be laid out. The first battery of tests would consist of a feed stream of pure hydrogen to establish a baseline. If the first test were successful then,

subsequent tests would be run with binary mixtures of nitrogen-hydrogen and carbon dioxide-hydrogen. Finally, ternary mixtures of all three gasses in various compositions would be tested. With this data, important membrane characteristics would be calculated. These include: n-factor, hydrogen selectivity, and activation energy. Finally, the variations in these characteristics would be compared to predictions by models and experimental results found in literature.

Initially, certain precedents were set that became constants throughout the entirety of the study. During the heating and cooling phases that bounded each experimentation session, the palladium membrane under investigation was exposed to an inert environment. This was accomplished by the opening of the facilities cross connect valve, allowing argon to bath both sides of the membrane. Special care was always taken to ensure minimum hydrogen exposure below 300 Celsius. From literature, exposure of palladium to hydrogen at sub-300 Celsius temperatures is known to cause embrittlement, which leads to membrane failure [3]. The initial test was conducted at 350 Celsius. This temperature was picked for the first test because it was in the midrange of the temperatures to be investigated. This study was looking into steady state operational characteristics of each membrane. Thus, the amount of time, if any, to reach a steady state condition needed to be found. Once the 350 degree Celsius temperature was reached, the cross connect valve was closed and the argon isolated to the sweep side of the membrane. The pure hydrogen feed stream was energized and analysis began with the gas chromatograph (GC). From literature it was learned that permeation should begin instantly and remain relatively constant; however, a steady state test was run to ensure similar behavior under this study's

conditions. Three permeate samples were taken every fifteen minutes for three hours. The results showed that steady state was reached within the first few samples; however, after about a half an hour there existed a noticeable increase in permeation. There were several possible explanations for this: perhaps there were non-negligible transient effects at play, the new membrane may have initial surface contamination that was being removed by the hydrogen flow at elevated temperature, or there might be an error in the facility. The answer came after close inspection of the facility. The temperature of the membrane, housing, and gas were assumed to be equal to the temperature returned by the thermocouple embedded in membrane housing. During the heating phase, the temperature indicated by an installed thermocouple lagged the set temperature display of the furnace. As such, the first experiment commenced once the membrane thermocouple reached the desired temperature. At this point it was found that, while the furnace display continued to read the set point temperature, the housing display would slowly creep up over time. Through trial and error, it was found that the furnace temperature needed to be set about ten to eleven degrees below the desired temperature. It is to be noted that while diffusion is not explicitly a function of temperature according to Sievarts' law model, temperature affect the diffusion rate and the activation energy. Once this was discovered, the next test saw not only a constant system temperature but also hydrogen flux.

There were several other discoveries learned in these initial tests. Among them, it was realized that the CG's analysis rate was 10 second plug of gas about every three minutes. This meant that any investigations of short timescale processes would not be practical. In addition real time analysis would also not be possible.

Another experimentation rate limiting factor was found to be the furnace heating and cooling rate. While the pressures studied could be changed with a quick turn of a knob, the switching from one testing temperature to another was much more time consuming. As a result, experimental efficiency could be optimized by running as many tests as possible at one temperature before attempting experiments at another. It is also important to note that the CG does not pick up argon, the percentage of argon is assumed to be the mole percent that remains absent from the GC's output. For example if the CG reports a sample of 10% hydrogen, 5% carbon dioxide, and 5% nitrogen, the argon level was assumed to be 80%.

With an established baseline emplace it was time to test the various compositions of simulated syngas. The same heating phase procedures were followed as before until the desired operational temperature of 400 Celsius was reached. The first battery test would consist of a binary mixture of nitrogen and hydrogen in a 1:2 molar ratio. The first battery of tests consisted of five samples taken at each 10, 20, and 30 psi. The exact same tests were then repeated the following day to compare results. The first thing that was noticed during data analysis was that there was a significant difference between the two days. It took a very thorough review of the test procedure; it was found that the sweep gas flow rate was not kept constant. While setting up for the experiment, much care was taken in ensuring the feed stream input was controlled and accurate, not much attention was paid to the sweep side. The thought was that the purpose of the sweep side was to keep the permeate side partial pressure low and bring permeated hydrogen gas to the GC. The issue was that when the GC analyzed the gas stream, it was only sampled a fraction of the gas that flowed

into it. This meant that the molar percentage data returned by the GC reflected the relative molar percentages in the sample. The absolute value of the hydrogen flux would be relative to the absolute flow rate of the sweep gas set by the mass flow controller. Therefore, if the sweep gas flow rate was not kept constant, the permeation would be diluted and a different hydrogen flux would be calculated. The second thing noticed in the experiments was trace amounts of nitrogen, oxygen, and carbon dioxide. From the work done by James et al., it was known that the membranes studied prior had compromised membrane layers. This lead to a strong nitrogen presence in the permeate [90]. While a defective membrane layer was possible, it would not explain the oxygen and carbon dioxide. The sweep side of the membrane facility was always maintained at 3 psi. This positive pressure system was maintained not only to negate any leaks but also to provide the GC with the required sampling pressure. If there was an air leak one would expect to see a 3.76 nitrogen to oxygen ratio. Rather, the ratio given by the GC was on the order of 2.95 nitrogen to oxygen. Further, if there was a leak in the palladium membrane, one would expect to see a nitrogen to oxygen ratio greater than 3.76. Looking back at the pure hydrogen case, the presence of nitrogen and oxygen carbon dioxide was also found. Next test results were looked at to determine whether there was any variation in the permeate stream impurities as a function of either temperature or pressure. Analyzing the results showed a slight rise in the nitrogen detected with a rise of pressure. Later, it would be found that there was a very slight decrease in the nitrogen detected with rise in temperature; however, this decrease was negligible.

To address this issue of the unexplained gas reading, effort was turned toward the GC. As discussed earlier, the operator's manual did not address the accuracy of the machine. The GC calculates concentration by measuring the time molecules take to travel through its separation columns. This time is a reflection of the mass of the molecule. Molecules are identified by comparing the time data to that of known molecules. The quantity is determined by and integration of the mass signal over the amount of time that substance is detected. An attempt was made to bake-out and recalibrate the system however the trace impurities remained. Comparing the results of each analysis, it was seen that the except for the slight change in the level of the non-hydrogen feed gas component, the trace levels remained statistically the same throughout all experiments. Thus, for the remainder of this study the trace gasses were taken as a bias error in the GC. For experiments where one of the trace gasses was also an element of the feed stream, the bias for that gas was subtracted from the amount of that gas returned by the GC. This determined the significance other feed stream components present in the sweep stream. Further discussion of membrane leaking and hydrogen selectivity will be explored in the next section.

Despite the concerns pertaining to sweep gas flow rate and extra gasses in the GC analysis, one element was present in every permeation test: hydrogen. The following are results of the syngas composition experiments.

All experiments were conducted in the same manner with care to ensure that all parameters remained the same throughout each experiment. The syngas compositions tested include: binary compositions of nitrogen-hydrogen and carbon dioxide-hydrogen. Both mixtures were studied in molar ratios 1:1 and 1:2. Two

ternary mixtures of hydrogen-nitrogen-carbon dioxide was also tested. Their molar ratios were 1:1:1 and 2:1:1. These mixtures were chosen because the partial pressure of hydrogen would be equal in both the binary ternary tests, thus directly comparable. Each mixture was studied at temperatures of 325, 350, 375, and 400 Celsius and total pressures of 10, 20, and 30 psi. The studied temperatures and pressures were initially chosen because they spanned the operational design limits of the experimental facility and membrane. When the data was analyzed, it was found that the trend line was linear with an R^2 value above 0.99. As a result, no intermediate data points were taken for the remaining studies. Temperatures and pressures above and below the ones studied here are recommended for future investigation. The argon sweep gas was maintained at 100 mL/min, and used with the membrane surface area to calculate permeate flux. For each experiment 3 to 6 samples were taken over the course of about15 minutes. Figure 4-2 shows the effect of temperature on a 1:1 binary mixture of hydrogen-nitrogen.

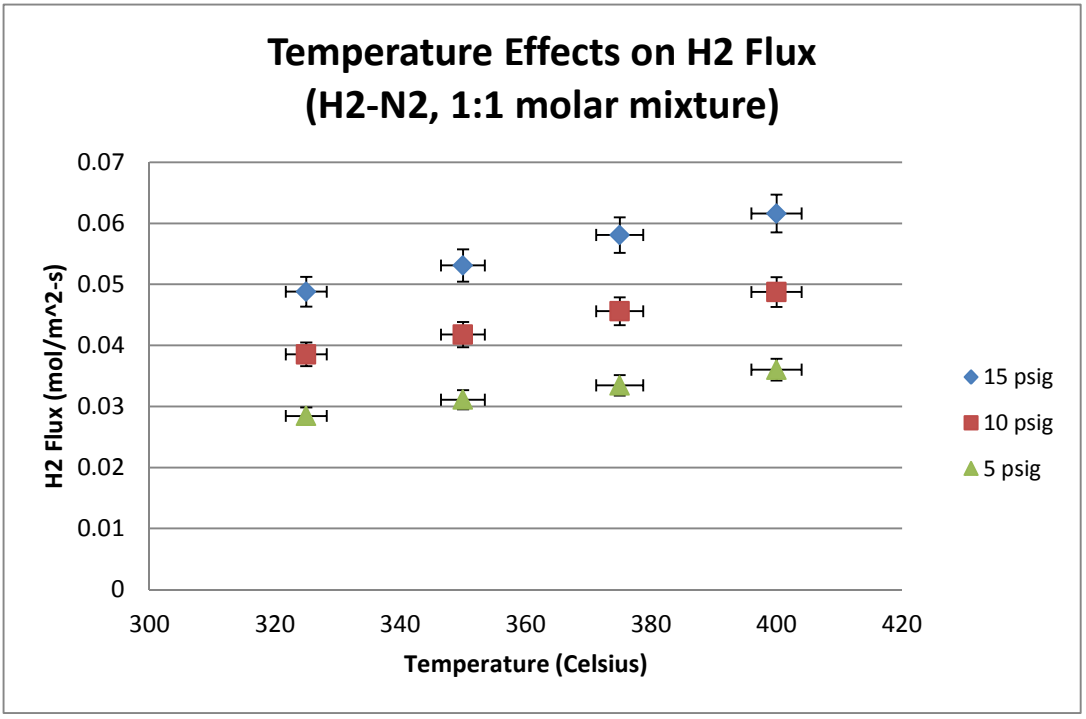

Figure 4-2. Temperature effects on permeation: comparison of hydrogen permeation as a result of temperature change at three constant partial pressures of H_2 in a 1:1 molar H_2-N_2 binary mixture.

Previous literature reveals that temperature has an effect on hydrogen permeation, though a relatively small one [3]. As mentioned before the temperature effects, while not obvious in the Sievert's model, shows up in the diffusion coefficient and activation energy. Figure 4-3 shows that for all pressures tested a general upward trend in hydrogen permeation was realized with increase in temperature, which agrees with literature [3]. Results show that, over an increase in temperature from 325 to 400 Celsius, the membrane displayed a permeability increase of around 26%. It is also interesting to note that not only did the permeation increase slightly with the temperature, but also its rate of increase grew.

That data would be necessary to determine if the trends seen in this study would continue for other operating conditions. Pressure had the greatest effect on hydrogen permeation. Figure 4-3 shows that for three temperatures tested, results

showed a strong upward trend in hydrogen flux with increase in temperature. This is in good agreement with the available results in the literature [3]. Over an increase in hydrogen partial pressure from 5 to 15 psi, the membrane permeability increased by over 71%. As seen from the role of temperatures, the rate of increase in permeation also appeared to increase with the rise in pressure. Thus, higher pressures (and also higher temperatures), help support high membrane permeability; however, increasing pressure exhibited a much greater effect at increasing overall hydrogen permeation.

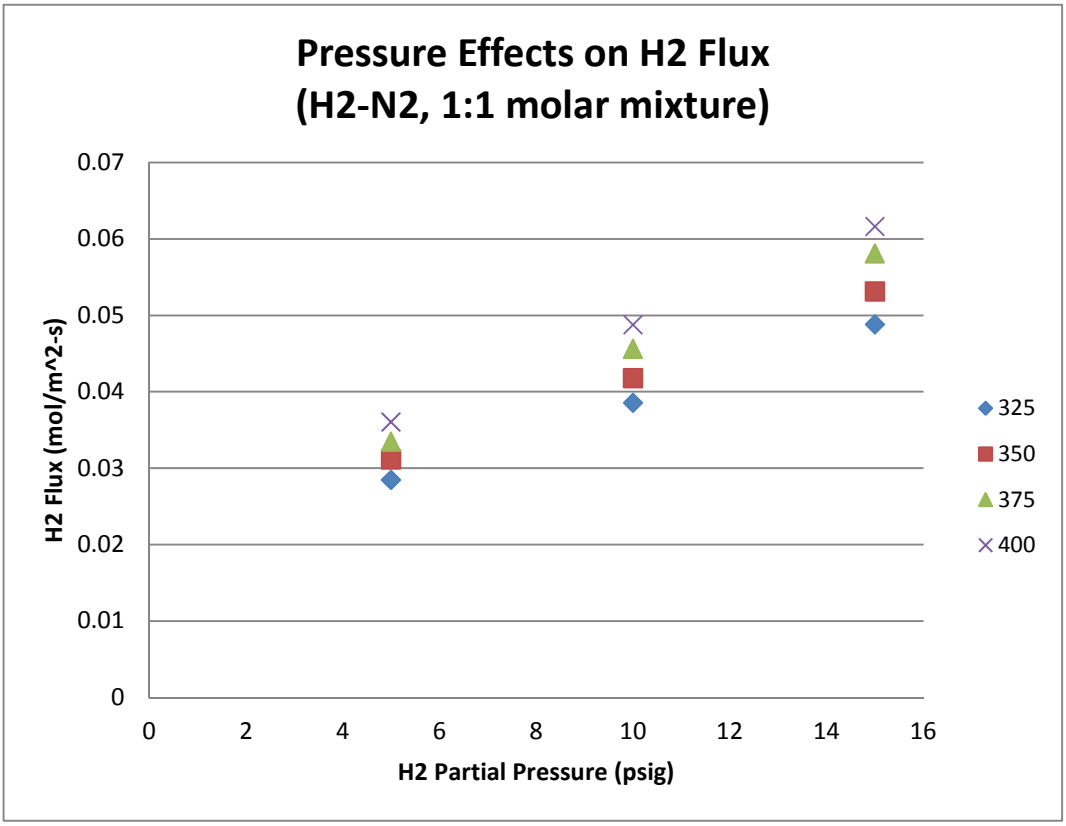

Figure 4-3. Pressure effects on permeation: comparison of hydrogen permeation as a result of pressure change at four constant temperatures of H_2 in a 1:1 molar H_2-N_2 binary mixture.

As per Fick's Law, the partial pressure of a gas governs its ability to diffuse through a metal. Likewise, the syngas composition with respect to its ratio of hydrogen played an important role in determining permeation. Binary and ternary gas mixtures of hydrogen and nitrogen, and hydrogen and carbon dioxide were examined in this study. Intuitively, the experimental results showed that syngas with a 50% relative partial pressure of hydrogen significantly outperformed syngas containing only a 33% relative hydrogen partial pressure for the same total feed pressure. What was not expected was that the feed stream with the higher partial concentration of hydrogen also outperformed the one with lower concentration when the partial pressures of hydrogen were equivalent. Figure 4-4 and 4-5 show hydrogen permeation results comparing feed gasses of different compositions.

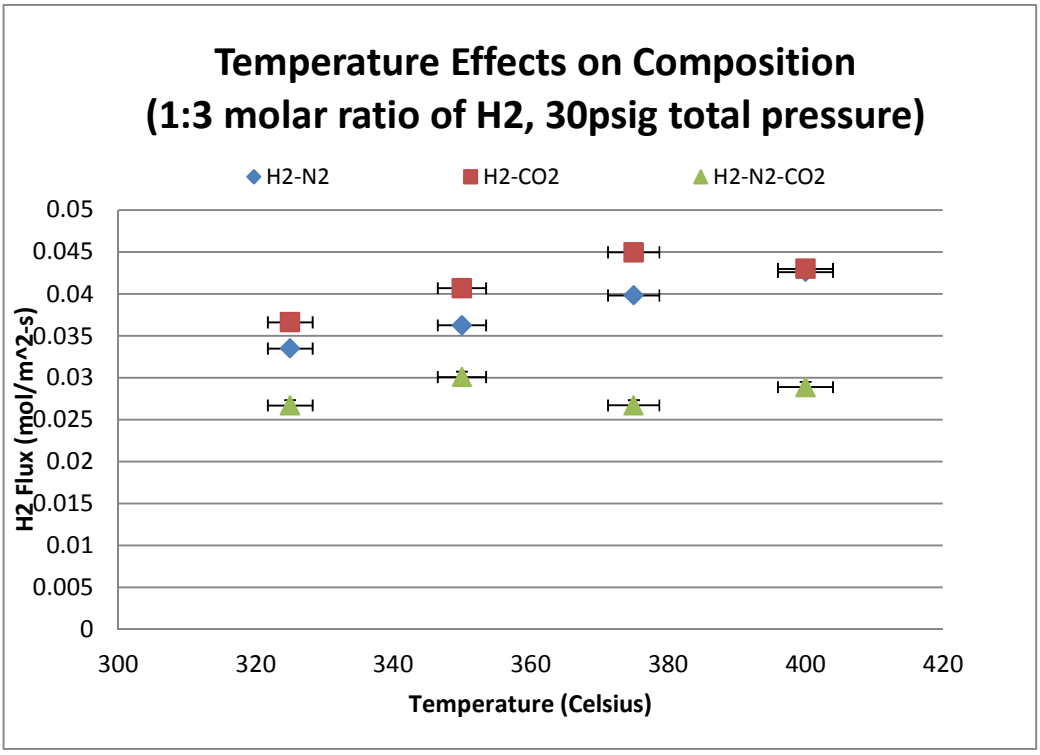

Figure 4-4. Temperature effects on three feed gas compositions. H_2 is in a 1:2 molar ratio with the remaining component(s).

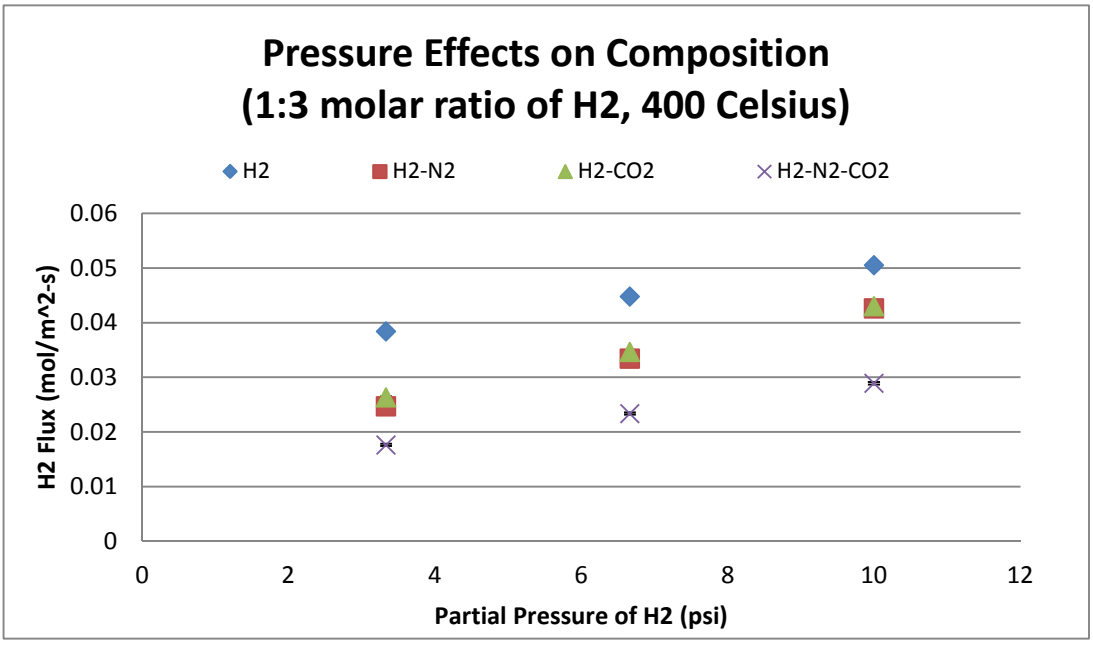

Figure 4-5. Pressure effects on three feed gas compositions. H_2 is in a 1:2 molar ratio with the remaining component(s). Pure H_2 stream is shown for reference.

4.2.2 Investigation of Membrane Defects

During experimentation, syngas components, other than hydrogen, appeared on the permeate side of the membrane. It is well known that hydrogen is the only syngas component capable of diffusing through palladium. The system was operated at positive pressure, ruling out intrusion from the environment. The design of the membrane housing prevented gasses from leaking around membrane, yet the gasses were present. This pointed to a compromise in the actual membrane surface. While the amount of errant syngas components that appeared on the permeate side of the membrane was very low (< 0.5% of the permeate stream), an understanding of the physics involved was important. To quantify the effect of the defects on hydrogen permeation, one could not assume the leakage would occur in the same ratio as the syngas mixture. In fact, the type of diffusion witnessed in this incidence was likely

Knudsen diffusion. Knudsen diffusion is the process in which individual molecules diffuse through an opening of channel in which the length scales are on the order of the mean free path. The equation for Knudsen diffusion, $D_{K,}$ is given as:

$$D_K = \frac{d}{3}\left(\frac{2k_B T}{m}\right)^{\frac{1}{2}} \tag{4-1}$$

where d is the pore diameter, k_B is Boltzmann's constant, T is temperature, and m is molecular mass. Note that the gas flow is inversely proportional to the square root of its molecular mass. Based on Knudsen diffusion, Thomas Graham discovered an empirical relationship between the gas mixtures and their leakage rate called Graham's Law of Effusion [97]. Graham's law states that the rate of effusion of a gas is inversely proportional to the square root of the mass of its particles [97]. Thus, in a binary gas mixture, like the ones in this study, one can find the effusion rate of one gas (hydrogen) from the known effusion rate of the other (nitrogen/carbon dioxide) using:

$$Rate_1 = Rate_2 \times \sqrt{\frac{mass_1}{mass_2}} \tag{4-2}$$

where, $Rate_1$ and $Rate_2$ are the effusion rates of each gas and $mass_1$ and $mass_2$ represent the molar masses [98]. According to Graham's Law Hydrogen in the presence of nitrogen and carbon dioxide should leak at a ratio of 3.72:1 and 4.67:1, respectively. The hydrogen permeation is calculated by multiplying the carbon dioxide effusion by the effusion factor, 4.67 and subtracting that product from the total hydrogen detected in the permeate side. The rate of effusion increased much slower than did the rate of permeation.

Whatever the cause of this diffusion, the appearance of non-hydrogen species on the permeate side of the membrane factor into the membrane's "selectivity." The selectivity is merely the hydrogen permeation flux divided by the flux of the other feed species [67]. Selectivity values for several syngas composition experiments may be seen in table 4-1. Figure 4-6 displays the trend in selectivity as a function of raising pressure and temperature.

Selectivity (1:2 molar ratio of H2:CO2)				
	Temperature (Celsius)			
Partial Pressure of H2 (psig)	**325**	**350**	**375**	**400**
3.3	113.4	181.6	268.9	188.8
6.7	95.1	145.8	206.8	146.7
10.0	72.0	115.2	166.5	111.5

Table 4-1. Selectivity values for a syngas mixture with a 1:2 molar ratio of H_2-$CO_2$for various temperatures and pressures.

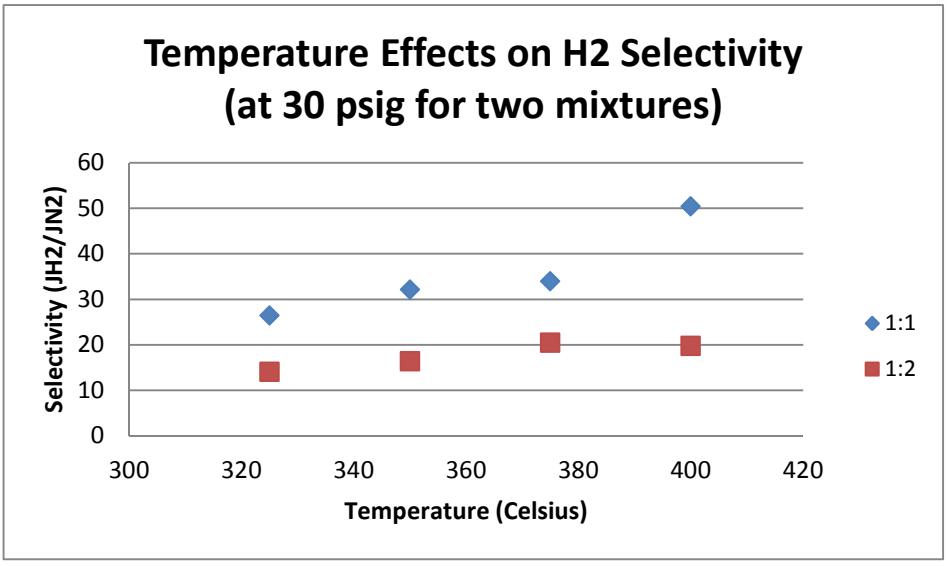

Figure 4-6. Temperature effects on two different compositions of H_2-N_2 at a total pressure of 30 psig (the H_2-N_2 ratio is shown).

The increasing selectivity can most likely be attributed to the expanding of the membrane and housing causing as tighter fit and allowing less nitrogen to leak by. The contrary is true for the rising pressure, where there was a decrease in selectivity due to increased leakage.

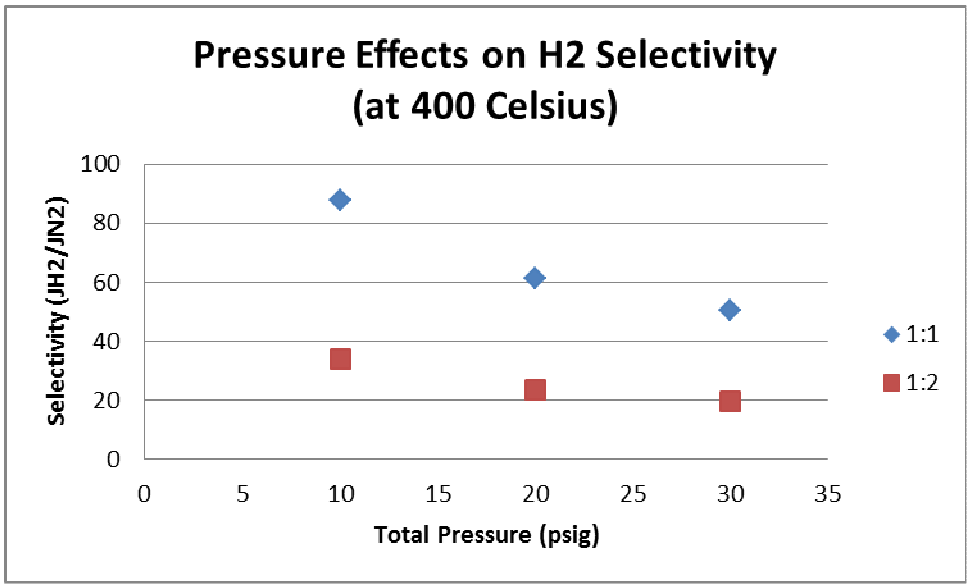

Figure4-7. Pressure effects on two different compositions of H2-N2 at 400 Celsius (the H2-N2 ratio is shown).

4.2.3 Composition effects on Pressure Exponent and Activation Energy

Once the permeation experiments had been run and data gathered, it was time to determine n-value or pressure exponent for the membrane. The n-value comes from Sievert's Law see in equation (2-8). It is known that the hydrogen permeation flux goes as the difference in the partial pressures raised to the one half. As discussed before, n = 0.5 is an ideal case that only takes bulk diffusion into account. That being said, if any other process acts to limit the bulk diffusion transport mechanism then, n > 0.5. While this does not account for the physics, this quantity is used by researchers to describe membrane performance. The pressure exponent was arrived at using the

procedures developed by James et al. To ensure an accurate trend, additional pressure data was collected at the temperatures tested. For this set of experiments, the molar hydrogen permeation flux, J_H, and the difference hydrogen partial pressures were tabulated in Microsoft Excel. Next the data were imported into Engineering Equation Solver where the data were plotted and a power law curve fit was done to return the n value. One of these plots can be seen in figure 4-8.

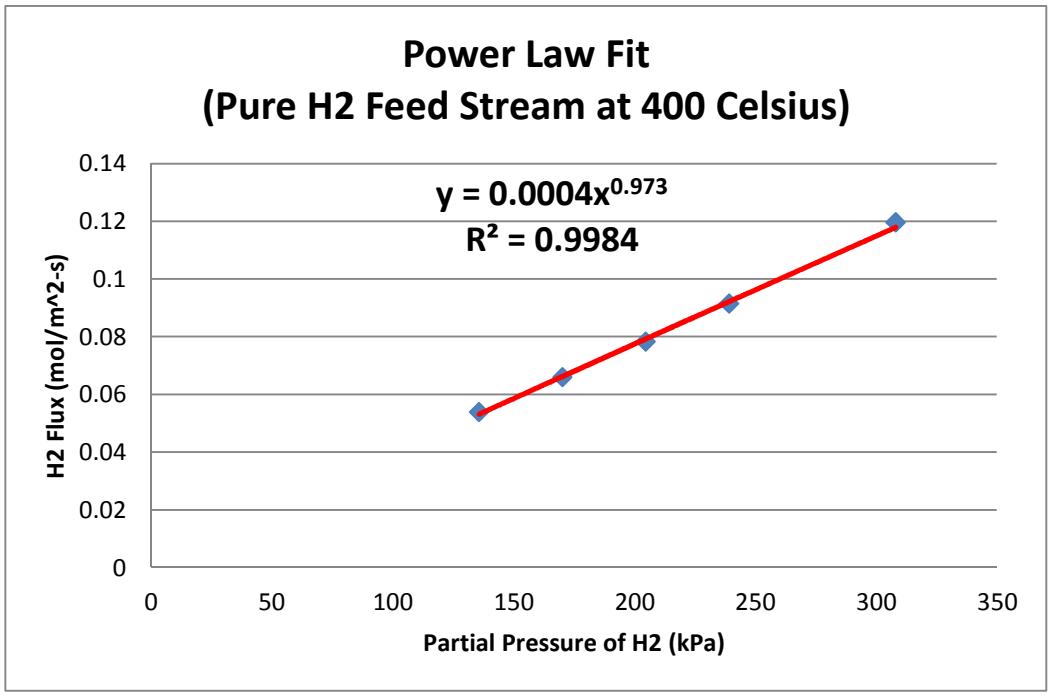

Figure 4-8. Power law fit to find pressure exponent values.

All the n-values calculated were greater than 0.5. This communicated that there was more affecting the hydrogen permeation rate than just bulk diffusion. From the work reviewed earlier, the rate limiting factors likely included surface effects on the upstream surface possibly due to active site competition by the other gas components. The downstream surface could have been possibly affected by negative

interaction at the interface with the porous support. Flow resistance within the porous stainless steel may have been a factor, too.

The other piece of information learned from the regression analysis was the leading coefficient in the curve fit equation. Looking back at equation (2-6) one can see that the leading coefficient from the EES data corresponds to the diffusion coefficient, D_K, and Sievert's Constant, K_s. from literature D_K and K_S can be combined into the permeability term, k, shown below [15,66]:

$$\alpha = D_K K_S = k = k_0 \exp\left(-\frac{E}{RT}\right) \tag{4-3}$$

Where k_0 is the permeability constant, E is the activation energy, and R is the ideal gas constant. If we plug equation 4-3 in to equation 2-6, we get,

$$J_H = \frac{k_0}{2l_m} \exp\left(-\frac{E}{RT}\right)\left[p^n_{H_2,upstream} - p^n_{H_2,downstream}\right]. \tag{4-4}$$

To get the activation energy, equation (4-4) must be rearranged so that the molar flux can to be plotted versus inverse temperature. When this is complete, a linear regression can be done on the plot as shown below.

$$\ln\left(\frac{J_{H_2}}{\Delta P}\right) = -\frac{E}{R}\left(\frac{1}{T}\right) + \ln\left(\frac{k_0}{2l_m}\right), \tag{4-5}$$

Mirroring:

$$y = mx + b \tag{4-6}$$

Reveling:

$$y = \ln\left(\frac{J_{H_2}}{\Delta P}\right) \tag{4-7}$$

$$m = -\frac{E}{R} \tag{4-8}$$

$$x = \frac{1}{T} \tag{4-9}$$

$$b = \ln\left(\frac{k_0}{2l_m}\right) \tag{4-10}$$

One of these plots can be seen in figure 4-9 and 4-10, while a table of calculated activation energies for various experiments can be seen in table 4-3.

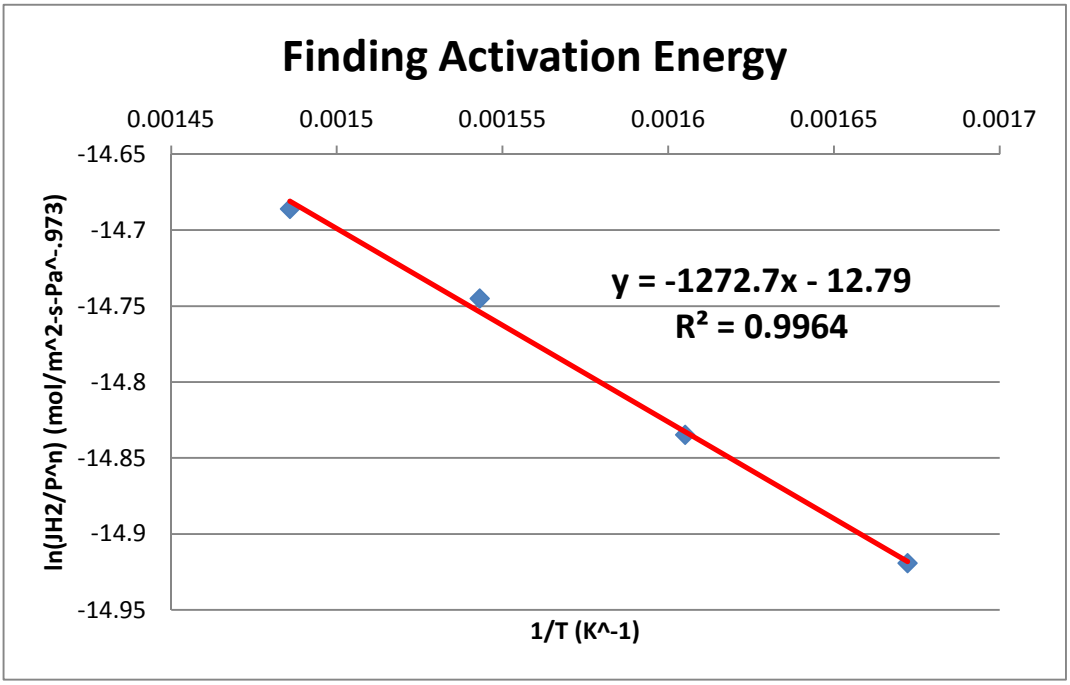

Figure 4-9. Linear regression to find activation energy.

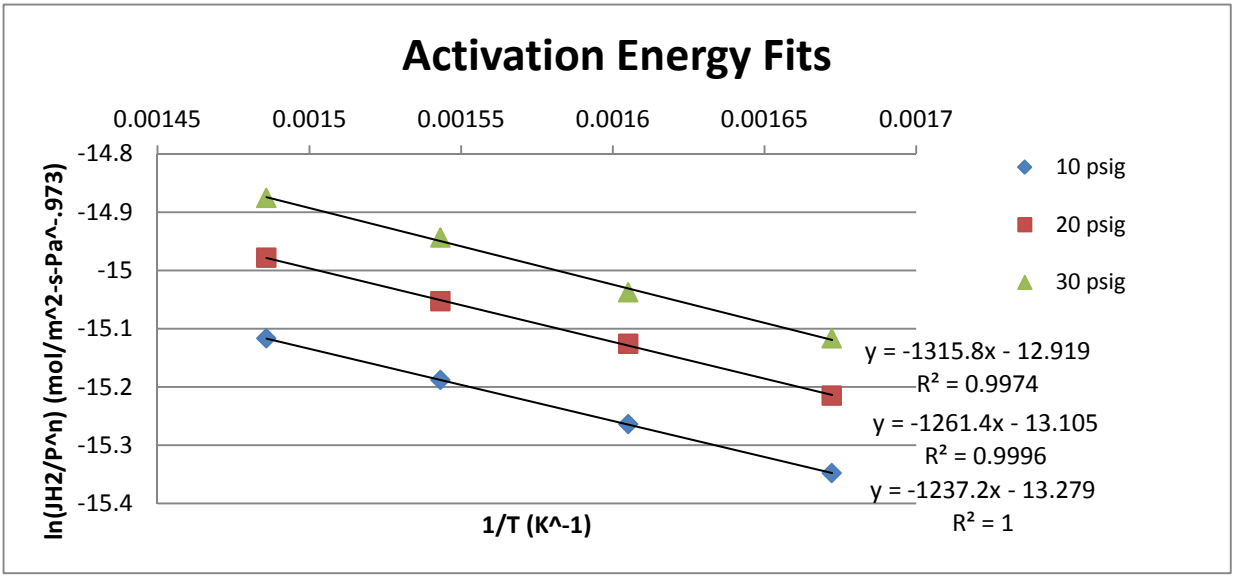

Figure 4-10. Activation energy fits for a 1:2 molar H_2-N_2 mixture. Notice how the trend lines stay relatively parallel and the pressure changes the intercept which is related to k_0.

Total Pressure (psig)	*H_2-N_2 (kJ/mol)*	*H_2-CO_2 (kJ/mol)*
30	10.94	13.24
20	10.49	13.66
10	10.29	12.85

Table 4-3. Calculated activation energies from various experiments (1:2 molar ratio).

4.2.4 Comparison to Literature

This study would not have been as successful without guidance from literature and the previous work done and procedures laid down by James et al.. One of the most interesting outcomes of this study was seeing how the experimental results of this study compared to that of literature. As there were challenges faced while executing this study, there were also challenges faced in comparing its results. It immediately evident that there were as many different ways to express hydrogen flux as there were researchers studying it. From this exercise of converting results from

many different sources, the importance presenting of standard forms of data was learned. Standardizing data when possible makes it more accessible to other researchers, aiding in the progress of the subject area. Table 4-3 lists outcomes comparisons of pressure exponent.

Membrane Thickness, lm (μm)	*Activation Energy, E (kJ/mol)*	*Source*
10	12.72	This Study
12	28.13	James et al. [90]
13	10.7	Uemiya [66]
6	19	Huang [106]
15	13	Huang [106]
20	10	Huang [106]
10	7.1	Wang [86]
130-729	18.56	Davis [99]
11,500	13.46	Toda [100]
10-150	11.92	Hurlbert et al. [102]
486-762	15.67	Koffler et al. [103]
800-2025	12.81	Holleck [101]
100-1000	15.46	Balovnev [104]
940	20.5	Katsuta et al. [105]
1000	13.81	NETL [15]
1000	13.41	NETL [15]

Table 4-3. Comparison of activation energies.

Chapter 5: Conclusions and Recommendations for Future Work

5.1 Conclusions

In this study binary and ternary mixtures of hydrogen, nitrogen and carbon dioxide were investigated. The hydrogen permeation results gathered in this study supports that found in the literature. For each composition, increases in pressure and temperature resulted in increased hydrogen flux. Consistent with Sievert's Law, pressure was shown to play the dominant role in each case. Nevertheless, results showed that even with the difference in the partial pressures of hydrogen held constant, hydrogen flux decreased with a decrease in the relative concentration of hydrogen in the simulated syngas. Among the binary mixtures, carbon dioxide displayed a greater effect on hydrogen permeation than did nitrogen. Comparing the binary mixtures to the ternary mixtures, the feed stream of nitrogen was shown to have the highest permeation flux and the ternary mixtures lowest. Over the course of the study non-hydrogen species from the feed stream showed up in the permeate stream. Though the leaking accounted for less than 5% of the permeate, the physics governing the mechanics of the leaking species was investigated.

A comprehensive calculation of the pressure exponent and activation energy was completed. In all cases the exponent was found to be larger than 0.5. This was especially evident when comparing the pure hydrogen tests to the simulated syngas. This supports that composition of the syngas plays a large role in determining the rate limiting processes. As the concentration of certain species increases, there likely

exists competition for the available active sites on the surface of the membrane, this in turn drives up the influence of surface effects and thus the pressure exponent.

This study has shown that the composition of the feed stream greatly affects hydrogen permeation. Understanding the effects that various species within a syngas have on hydrogen permeation will be critical to designing effective membrane reactors.

5.2 Recommendations for Future Work

As this study evolved, many ideas for future investigations arose. These are outside the scope of the present research and are therefore listed here in this chapter as recommendation for future work. This chapter provides possible improvements to the experimental facility and the opportunities for worthwhile future investigations.

5.2.1 Hydrogen Separation Facility Improvements

Throughout this study the membrane housing performed beautifully. The only improvement would be to create a better seal around the outside of the membrane. Due to the housing's design and the membranes' geometry, gas would leak radially from the porous stainless steel. A better seal would allow for experiments to be done below atmospheric pressure. The hydrogen separation facility worked well and was very user friendly. However, there are a few modifications that would improve performance. Currently, the feed gas is vented after passing through the membrane. An improvement would be the addition of a line that could be directed to the GC (gas chromatograph) to investigate the amount of hydrogen that was being removed from

the feed stream. Similarly, a permanent line should be added to direct the feed gas to the GC prior to the membrane. Before each composition experiment was conducted the feed stream was tested to ensure an accurate mixture. This involved rearranging the feed stream tube prior to each day's work. A permanent line would cut down on labor and lower the risk of leaks. Finally, these new lines should be combined in a manifold with permeate line so that a simple twist of a valve would allow the future researcher to select which gas stream would be sampled by the GC.

5.2.2 Future Experimental Work

Throughout the study there were several interesting results and questions that arose and are recommended for future investigation. The effect of the feed stream flow rate over the membrane was not examined in this study. The effect that the flow rate has on the hydrogen's ability to adsorb on the membrane's surface would be useful information for industrial application. There were interesting data collected at the 400° C temperature point involving a dip in hydrogen selectivity. This temperature effect on hydrogen selectivity should be further investigated in greater detail. Furthermore, temperatures and pressure outside of the ones examined in study should be investigated to discover if and how the permeation trends continue.

Arguably the most critical element of this study was the membrane. According to literature, pure palladium is expensive and many advances have been made using palladium alloys to great effect. The next experimental effort should study thin palladium-alloy membranes. Specifically, palladium-copper membranes with copper concentrations above 40% and palladium-silver membranes with silver concentrations of 20-40% should be examined. These alloys showed performance

characteristics greater than that of pure palladium under similar conditions [10,35,36,46,47].

There was an extensive lead time on replacement membranes. An excellent area for future work would include the collaboration with a materials lab for the manufacture of the membranes. This would allow for a better study of how palladium thickness and alloys effects permeation. Studies should be carried out on other types of membranes, such palladium silver and palladium copper that offer much lower costs than pure palladium membranes. In addition, new membrane geometries could be investigated and optimized for use in gasification processes. In this study the disk geometry was optimal for making the one-dimensional and steady state assumptions to discover the membrane's performance properties. However, to study membranes for practical hydrogen separation other geometries such as an annulus would be more effective.

Similarly, research should be continued with syngas composition to include the other gas species that are known to be present in the actual syngas. This includes CH_4, O_2, H_2O, CO and H_2S. Most gasses may be run on the current facility without modification; however, the changes would be necessary for H_2O, CO and H_2S. CO and H_2S present significant safety concerns. By running experiments in a fume hood or otherwise improved ventilation, this type of investigation would be possible. To modify the facility to study the effects of water in the feed stream, a steam generator and high temperature mass flow controller would need to be added upstream of the membrane. In addition, sufficient heating or insulation would need to be added to the tubing to ensure the water remained in the gas phase. The other feed stream

components would have to be preheated so that the steam would not condense during mixing. Finally, the water would need to be separated downstream of the membrane and prior to entering the GC. This could be accomplished via heat exchanger to condense the majority of the water followed by a moisture absorber. This is necessary because water can negatively affect the GC. An examination of these species is imperative for future technology development on hydrogen separation. There is significant evidence in the literature that these gases have an even bigger effect on the surface chemistry involved in hydrogen permeation. Finally, experiments should be done with actual syngas samples produced in the combustion lab by the concurrent gasification studies. It would be very interesting to see how the novel membranes stand up to genuine conditions vice the simulated syngas.

Finally, the ultimate desire is to collect a pure hydrogen gas. A sweep gas was very useful in ensuring the low partial pressure of the hydrogen on the permeate side of the membrane, in turn, allowing maximum hydrogen permeation. However, in a practical application the argon may be difficult to separate. Thus, experiments should be conducted to include sweep gasses separation. One option for this would be to modify the facility to also run steam as a sweep gas. Steam could be easily cooled and condensed out of the sweep stream, leaving the desired pure hydrogen gas. In industry, waste heat from power generation could be utilized to create the steam for this process.

5.2.3 Future Modeling Work

One of the most interesting areas of permeation research is the modeling effort. Here efforts could focus on creating a more detailed permeation model with

the desired flexibility on input and operational parameters. A flexible and detailed model would help guide the researcher in making informed decisions on the type of membrane to be built for each application. This could help reduce expensive experimental efforts and also help gain a better understanding of the mechanisms that govern hydrogen permeation through palladium based membranes.

Temperature and Pressure Effects on Hydrogen Separation From Syngas

Aaron B. Leyko

Ashwani K. Gupta[1]
Distinguished University Professor
e-mail: akgupta@umd.edu

Department of Mechanical Engineering,
University of Maryland,
College Park, MD 20742

Multicomponent synthetic gas (syngas) mixtures produced from the gasification of coal, low grade fuel, wastes, and biomass offers a novel source of hydrogen production. Gasification also eliminates much of the pollutant emissions from the combustion these fuels. Palladium based membranes offer a promising method for extracting hydrogen from syngas. Experimental results are presented from a laboratory scale experimental facility. This facility was designed and built to examine various types of palladium and palladium alloy membranes for harvesting hydrogen from the syngas. The thin membranes (on the order of ~12 μm) examined were supported on porous stainless-steel. A mixture of pure gasses consisting of hydrogen, nitrogen, and carbon dioxide were used to simulate syngas of different composition. The specific focus was on evaluating the role of operational temperature and pressure of membrane on the separation efficiency of hydrogen. Results are reported at temperatures from 325 °C to 400 °C and pressures from 5 to 30 psi (gauge) for various concentrations of hydrogen in the gas mixture. Results showed permeation to increase by up to 33% with a 75 °C increase in temperature. Permeation increased by over 50% with an increase in partial pressure of hydrogen by only 10 psi. These results provide clean hydrogen recovery from syngas obtained from gasification and pyrolysis of wastes and biomass. [DOI: 10.1115/1.4024028]

Introduction

With increased concern over energy security, sustained supply of fossil fuels, and their effect on climate change and global warming, hydrogen based energy systems are more attractive than ever before. Wider availability and utilization of hydrogen based energy can help address concerns about energy security, global climate change, and air quality. Currently used hydrogen production methods are both energy intensive and expensive. Hydrogen produced from coal, biomass, wastes, and low grade fuels is via thermal conversion, such as pyrolysis and gasification. This reaction produces synthetic gas (syngas) comprised of primarily CO, CO_2, and H_2 [1]. A reliable method of separating the hydrogen from the syngas is critical. Selective diffusion uses noble metal and polymer based membranes to extract the hydrogen [2]. Operating conditions as well as output preferences are key factors in determining the preferred method. In this study, we examine selective diffusion from palladium based membranes to separate out hydrogen. The effect of operating conditions, such as, mixture composition, temperature, pressure, and permeate quality is examined. This is a choice separation method when the hydrogen is produced via gasification. Hydrogen permeation with a palladium based membrane using simulated syngas components is examined here under various conditions. By examining membrane behavior, a greater understanding of the governing processes can be attained to foster practical solutions for obtaining high purity hydrogen at high efficiency.

Theory

Permeation is defined as the transfer of a gas from the high pressure side of a solid nonporous material to the low pressure side of the material. It is also important to note that permeability strictly refers to the rate of permeation through a solid material and not through pours or holes in the material [3]. Hydrogen permeation pathway through the palladium-based membrane consists of three steps. First, a reaction takes place on the upstream surface of the membrane, which disassociates the hydrogen molecules into hydrogen atoms. Second, the hydrogen atoms diffuse though the bulk of the membrane. Finally, a second surface reaction takes place on the downstream surface where the hydrogen atoms combine into hydrogen molecules [4]. Hydrogen permeation tends to decrease in the presence of other gasses [4]. The dilution of the hydrogen in the feed gas lowers the partial pressure to cause a reduction in permeation. Hydrogen may also be depleted along the surface of a membrane if boundary layer forms in the flow. Chemical properties of other gasses can create competition for active adsorption sites on the surface of the membrane [4].

The permeation process is most commonly modeled by Fick's first law, where diffusive flux is related to the concentration under steady state conditions. The hydrogen flux is proportional to the concentration gradient; the flux of hydrogen atoms through the membrane (J_H) is given by [4]

$$J_H = -D_M \frac{\partial C_H}{\partial x}$$

where D_M is the diffusion coefficient of the membrane, and C_H is the concentration of hydrogen atoms.

We relate the hydrogen atom concentration within the membrane to the hydrogen partial pressure using the empirical relation known as Sieverts' law [4]:

$$C_H = K_s p_{H_2}^{\frac{1}{2}}$$

where K_S is the Sieverts' constant, and p_{H_2} is the partial pressure of the hydrogen molecules. The hydrogen activity in solids a_H is defined as

$$a_H = \left(\frac{p_{H_2}}{p_{H_2}^{\circ}}\right)$$

where $p_{H_2}^{\circ}$ is the standard pressure of hydrogen. Putting partial pressure in terms of activity and substituting Sieverts' relation into Fick's law provides

$$J_H = -D_M K_S \left(p_{H_2}^{\circ}\right)^n \frac{\partial a_H}{\partial x}$$

Integrating over the membrane thickness provides

$$J_H = D_M K_S \left(p_{H_2}^{\circ}\right)^n \frac{a_{H,\text{upstream}} - a_{H,\text{downstream}}}{l_M}$$

If both the upstream and downstream surfaces of the membrane maintain equilibrium with their respective gas phase, then partial pressure can be substituted to give

$$J_H = D_M K_S \frac{p_{H_{2,\text{upstream}}}^{1/2} - p_{H_{2,\text{downstream}}}^{1/2}}{l_M}$$

Thus, the rate of hydrogen diffusion is proportional to the difference of the square roots of the upstream and downstream

[1]Corresponding author.

Contributed by the Advanced Energy Systems Division of ASME for publication in the Journal of Energy Resources Technology. Manuscript received March 1, 2013; final manuscript received March 8, 2013; published online April 29, 2013. Editor: Hameed Metghalchi.

partial pressures and inversely proportional to the membrane thickness.

Experimental Facility

A palladium membrane mounted on a porous stainless steel disk was used here. A palladium layer of 12 μm thickness was covered over the entire upstream surface of the stainless steel disk of nominal 1 in. diameter, 0.0625 in. thickness, and 0.2 μm pore size. The membranes were prepared at the Department of Mechanical and Chemical Engineering, North Carolina A&T State University (NC A&T).

The hydrogen separation setup consisted of basic control mechanisms and devices that incorporated both a feed mixture and a sweep gas. The system was designed for examining any combination of syngas that are characteristic gases from pyrolysis and gasification with special focus on wastes and biomass. The sweep gas flow was passed through both the feed and sweep side via cross-connect valve during heating and cooling operations to prevent membrane embrittlement. The gas mixture leaving the permeate side of the membrane housing was directed to a gas chromatograph for gas analysis.

Mass flow controllers (GFCs) having a flow range of 0–1000 mL/min were used. Controlled temperature electrical furnace (Carbolite single zone hinged tube) was used to examine the performance of membrane at the desired temperature. The facility allowed examination at up to 1200 °C furnace temperatures. A micro gas chromatograph (Micro GC) was used for gas analysis.

Experimental

Hydrogen permeation studies were conducted at various conditions of pressure, temperature, and gas mixture composition. In all experiments, the membrane was heated to above 300 °C in an argon atmosphere to prevent embrittlement [2]. Once the desired system temperature was attained, the sweep gas cross-connect valve was shut, limiting the flow of argon to the sweep side. The syngas supply valve was then opened to allow flow of the gas mixture. The membrane temperature was assumed to be equal to the temperature of the syngas and sweep gas at the membrane site since all were housed in the furnace maintained at the desired temperature. The mixture was monitored and controlled by the mass flow controllers, while system pressure was created via pin-valve adjustments downstream of the membrane. Once conditions were set, an initial sample was taken from the supply side upstream from the membrane to ensure the accuracy of the gas flow controllers. A series of readings were then taken from the permeate side consisting of a mixture of the sweep gas (argon) and any gasses that passed through the membrane. The sweep gas flow rate was set at a constant flow rate of 100 mL/min. This provided the sweep side of the membrane with a constant pressure (4 psi). It also provided the Micro-GC with sufficient pressure and flow rate, while ensuring a constant dilution of the permeated gas between experiments and comparable data. The Micro-GC does not provide direct measurement of argon. Instead, the Micro-GC only accounted for any permeate as a molar fraction of the gas sample. The remainder of the gas was not detected and assumed to be argon since hydrogen is only permeated from the membrane.

The baseline for the steady state behavior of the membrane was first established. After reaching the desired experimental temperature (taken from the thermocouple located in the membrane housing) and pressure for the system, permeation readings were monitored with the Micro-GC at about every 15 min to establish the time necessary to reach a steady state condition. The time to achieve steady state was found to be negligible relative to the sample rate of the Micro-GC.

Results and Discussion

The results obtained with the membrane heated at four different temperatures (325 °C, 350 °C, 375 °C, 400 °C) are now presented.

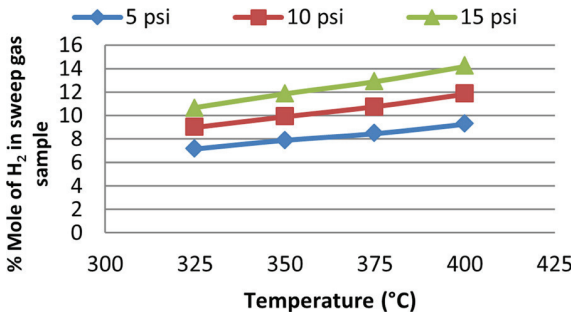

Fig. 1 Temperature effects on permeation: comparison of hydrogen permeation as a result of temperature change at three partial pressures (1:1 H_2:N_2)

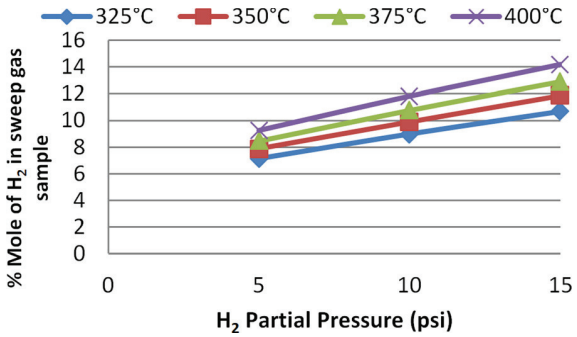

Fig. 2 Pressure effects on permeation: comparison of hydrogen permeation as a result of pressure change at four temperatures (1:1 H_2:N_2)

At each temperature, experiments were conducted at total syngas pressures in the range of 5 and 30 psi. These tests employed binary syngas mixtures of H_2 in N_2 or CO_2 at concentration ratios of 1:1 or 1:2.

Previous literature reveals that temperature has a small effect on hydrogen permeation [2]. Figure 1 shows that for all pressures tested, the hydrogen permeation increased with increase in temperature and pressure. These results are in good agreement with the prior results reported in the literature [2]. Results show that the membrane displayed a relative permeability increase of 29% to 33% with an increase in temperature from 325 °C to 400 °C.

Pressure had the greatest effect on hydrogen permeation. Figure 2 shows that for the three temperatures, hydrogen flux increased with an increase in temperature. With an increase in hydrogen partial pressure from 5 psi to 15 psi, the membrane permeability increased by nearly 50–53%. In addition, an increase in one factor (temperature or pressure) would magnify the effects of increase in the other factor. Thus, both higher pressures and temperatures help to enhance membrane permeability with an increase of pressure exhibiting a much greater effect on hydrogen permeation.

According to Fick's Law, the partial pressure of a gas governs its ability to diffuse through a metal. Likewise, the syngas composition with respect to its hydrogen content provided an important role on permeation. Binary gas mixtures of hydrogen and nitrogen or hydrogen and carbon dioxide were examined here. In both cases, experimental results showed that syngas mixtures composed of 50% H_2 significantly outperformed syngas containing only 33% for hydrogen. Figure 3 shows hydrogen permeation as a function of hydrogen concentration in the syngas.

Cylindrical membranes used here showed that gas flows along the surface of a membrane can create a boundary layer of low hydrogen concentration. This leads to a decreased hydrogen flux through the membrane due to the local drop in hydrogen partial pressure [4]. This investigation utilized a small, disk-shaped

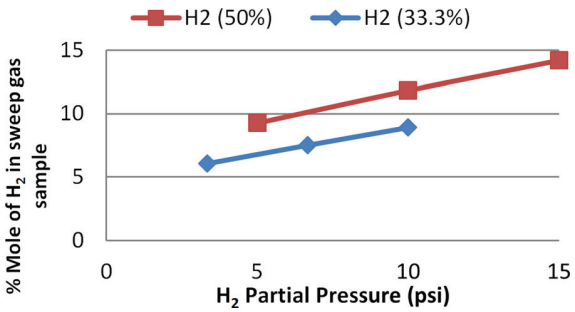

Fig. 3 Effect of mixture composition on permeation: comparison of pressure effects on hydrogen permeation at a constant 400 °C with a hydrogen-nitrogen mixture of two different compositions (H_2–N_2 syngas)

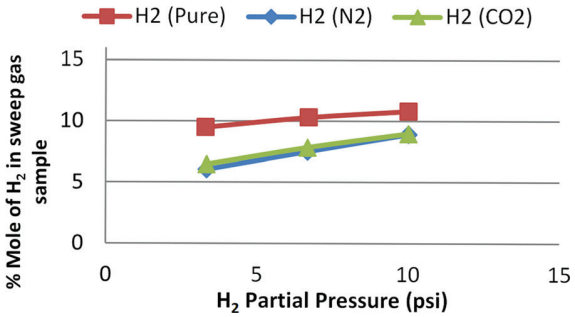

Fig. 4 Effect of mixture composition on permeation: comparison of pressure effects on hydrogen permeation at a constant 400 °C and partial pressure of hydrogen for pure H_2 and an 1:2 H_2–N_2 and H_2–CO_2 mixture (400 °C)

membrane and high syngas flow rate. Thus, loss in permeation due to the creation of concentration gradients was negligible. Examination of H_2–N_2 and H_2–CO_2 mixtures showed that hydrogen permeation is affected by the presence of other gasses [5]. A reason for this is thought to be the deposition and competitive adsorption of other gas molecules on the membrane's surface [5]. In the case of CO_2, the driving factors for this may include the formation of carbon monoxide and water from the reverse water gas shift reaction. Analysis of the membrane exhaust gas can confirm the presence of H_2O and the reverse water gas shift reaction. Negative effects on hydrogen permeation have shown decreased permeation with an increase in temperature in the presence of other gases and increased permeation with an increased concentration of other gasses [5]. The results found in the literature support the findings shown in Fig. 4, where one can clearly see the disparity between the pure hydrogen tests and the tests conducted with a syngas mixture for the same partial pressure of hydrogen.

During experimentation syngas components other than hydrogen began to appear on the permeate side of the membrane. Hydrogen is the only syngas component capable of diffusing through palladium. The system is operated at positive pressure, ruling out intrusion from the environment. Also, the design of the membrane housing prevent gasses form either side of the membrane from transporting to the other side. A close examination of the membrane itself revealed microscopic cracks on the palladium layer, possibly from repeated heating and cooling of the membrane. To quantify the effect of defects on hydrogen permeation, one could not assume the leakage would occur in the same ratio as the syngas mixture. Note that gasses flow through an opening is inversely proportional to its molecular mass. Graham's law of effusion provides a relationship between the syngas components and their leakage rate [6]. Effusion is the process in which individual molecules diffuse through an opening in a surface that is smaller than the mean free path. Graham's law states that the rate of effusion of a gas is inversely proportional to the square root of the mass of its particles [6]. Thus, in a binary gas mixture, like the one studied here, one can find the effusion rate of one gas (hydrogen) from the known effusion rate of the other (nitrogen/carbon dioxide) using

$$\text{Rate of Gas}_1 = \text{Rate of Gas}_2 \times \sqrt{\frac{\text{Mass}_2}{\text{Mass}_1}}$$

where, "Rate of Gas_1" and "Rate of Gas_2" are the effusion rates of each gas and "$Mass_1$" and "$Mass_2$" represent the molar masses [5]. According to Graham's law hydrogen in the presence of nitrogen and carbon dioxide should leak at a ratio of 3.72:1 and 4.67:1, respectively. Even with the high effusion factors for hydrogen, the results indicated effused hydrogen accounted for no more than 5% of the permeated hydrogen. However, results showed a rise in effusion with increased pressure and temperature. However, the rate of effusion increased much slower than the permeation.

The results have shown that higher flux of hydrogen in the syngas is favorable for enhanced permeation. Production of hydrogen-rich syngas can be accomplished using high temperature steam gasification as compared to gasification or pyrolysis [7,8], which combines some of the key attributes of high temperature air combustion technology [9,10] to generate high temperature steam at atmospheric pressure. The clean hydrogen produced can be used for many applications in energy and power for environmentally benign clean energy [11,12].

Conclusions

The hydrogen permeation increased with an increase in both temperature and partial pressure. These results are in good agreement with the data reported in the literature. Permeation is more favorable at a higher concentration of hydrogen in the syngas. The presence of defects in the membrane's palladium layer accounted for less than 5% of the total hydrogen flux. The results presented for 325 °C to 400 °C temperatures showed that an increase in temperature from 325 °C to 400 °C in the presence of N_2 or CO_2 increased permeation by up to 33%. Moreover, an increase in partial pressure of hydrogen from 5 to 15 psi with the same syngas composition increased permeation by over 50%. The results showed the presence of other gasses in the syngas had a strong effect on hydrogen permeation; however, pressure effect showed to be more dominant.

Acknowledgment

The authors gratefully acknowledge and thank Dr. Shamsuddin Ilias from the Department of Mechanical and Chemical Engineering at North Carolina A&T State University (NC A&T) and his research team for graciously providing the membranes used in this study. One of the authors (ABL) would also like to acknowledge and appreciate the financial support provided to him by the United States Coast Guard's Naval Engineering Postgraduate Program.

References

[1] Hingman, C., and van der Burgt, M., 2008, *Gasification*, Elsevier, New York.
[2] Grashoff, G. J., Pilkington, C. E., and Corti, C. W., 1983, "The Purification of Hydrogen: A Review of the Technology Emphasizing the Current Status of Palladium Membrane Diffusion," Platinum Met. Rev., **27**(4), pp. 157–169.
[3] Hunter, J. B., 1956, "Silver-Palladium Film for Separation and Purification of Hydrogen," U.S. Patent No. 2,773,561.
[4] Unemoto, A., Atsushi, K., Sato, K., Otake, T., Yashiro, K., Mizusaki, J., Kawada, T., Tsuneki, T., Shirasaki, Y., and Yasuda, I., 2007, "Surface Reaction of Hydrogen on a Palladium Alloy Membrane Under Co-Existence of H_2O, CO, CO_2, or CH_4," Int. J. Hydrogen Energy, **32**, pp. 4023–4029.
[5] Li, A., Liang, W., and Hughes, R., 2000, "The Effect of Carbon Monoxide and Steam on the Hydrogen Permeability of a PD/Stainless Steel Membrane," J Membr. Sci., **165**, pp. 135–141.
[6] Zumdahl, S. S., 2010, *Chemical Principles*, Houghton Mifflin, Boston.

[7] Ahmed, I., and Gupta, A. K., 2009, "Hydrogen Production Form Polystyrene Pyrolysis and Gasification Characteristics and Kinetics," Int. J. Hydrogen Energy, **34**(15), pp. 6253–6264.
[8] Gupta, A. K., 1996, "Thermal Destruction of Solid Wastes," ASME J. Energy Resour. Technol., **118**, pp. 187–192.
[9] Tsuji, H., Gupta, A. K., Hasegawa, T., Katsuki, K., Kishimoto, K., and Morita, M., 2003, *High Temperature Air Combustion—From Energy Conservation to Pollution Reduction*, CRC Press, Boca Raton, FL.
[10] Gupta, A. K., Bolz, S., and Hasegawa, T., 1999, "Effect of Air Preheat and Oxygen Concentration on Flame Structure and Emission," J. Energy Resour. Technol., **121**, pp. 209–216.
[11] Vellini, M., and Tonziello, J., 2011, "Hydrogen Use in an Urban District: Energy and Environmental Comparisons," J. Energy Resour. Technol., **132**(4), p. 042601.
[12] Braun, R. J., Hanzon, L. G., and Dean, J. H., 2011, "System Analysis of Thermochemical-Based Biorefineries for Coproduction of Hydrogen and Electricity," J. Energy Resour. Technol., **133**(1), p. 012601.

Bibliography

[1] R.G. Lemus, J.M.Martínez Duart, Updated hydrogen production costs and parities for conventional and renewable technologies, Int. J. of Hydrogen Energy 35 (2010) 3929–3936.

[2] I.A. Gomaa. "High temperature steam gasification of solid wastes: characteristics and kinetics" PhD Dissertation, University of Maryland, 2011.

[3] G.J. Grashoff, C.E. Pilkington, and C.W. Corti. "The purification of hydrogen: A review of the technology emphasizing the current status of palladium membrane diffusion." Platinum Metals Review 27 (4) (1983): 157-169.

[4] H.St.-C. Deville and L. Troost, Comptes rendus, 1863, 57, 965.

[5] H.St.-C. Deville and L. Troost, Comptes rendus, 1864, 59, 102.

[6] T. Grahm, Phil. Trans. Roy. Soc., 1866, 156, 399.

[7] S.C. Deville, H. Étienne (1818 - 1881). Scientific Identity. Dibner Library of the history of Science and Technology. Smithsonian Libraries Last accessed April 4, 2013, from http://www.sil.si.edu/digitalcollections/hst/scientific-identity/CF/display_results.cfm?alpha_sort=s

[8] L.J. Troost (1825-1911). Photo. Popular Science Monthly Oct. 1912.

[9] Graham, Thomas. Photograph. Encyclopædia Britannica Online. Web. 4 Apr. 2013. <http://www.britannica.com/EBchecked/media/38395/Thomas-Graham-engraving-by-C-Cook-after-a-photograph>.

[10] J.B. Hunter. "Silver-palladium film for separation and purification of hydrogen." U.S. Patent 2,773,561. 11 Dec. 1956.

[11] T.L. Ward, T. Dao, Model of hydrogen permeation behavior in palladium membranes, Journal of Membrane Science 153(2) (1999) 211-231.

[12] S. Wilke, M. Scheffler. "Potential-energy surface for H2 dissociation over Pd(100)." *Physical Review* 53.8 (1996): 4926-4932.

[13] A. Bhargav, "Model development and validation of palladium-based membranes for hydrogen separation in PEM fuel cell systems" Dissertation, University of Maryland, 2010.

[14] A. Unemoto, K. Atsushi, K. Sato, T. Otake, K. Yashiro, J. Mizusaki, T. Kawada, T. Tsuneki, Y. Shirasaki, and I. Yasuda. “Surface reaction of hydrogen on a palladium alloy membrane under co-exisence of H2O, CO, CO2, or CH4.” International Journal of Hydrogen Energy 32 (2007): 4023-4029.

[15] B.D. Morreale, M.V. Ciocco, R.M. Enick, B.I. Morsi, B.H. Howard, A.V. Cugini, and K.S. Rothenberger. “The permeability of hydrogen in bulk palladium at elevated temperatures and pressures.” Journal of Membrane Science 212 (2003): 87-97.

[16] F.J. Kong, J.G. Du, G. Jiang, The structure and potential energy function of PdCO molecule, Acta Physica Sinica 57(1) (2008) 149-154.

[17] N. Ozawa, N.B. Arboleda, H. Nakanishi, H. Kasai, First principles study of hydrogen atom adsorption and diffusion on Pd3Ag(111) surface and in its subsurface, Surface Science 602(4) (2008) 859-863.

[18] L. Semidey-Flecha, D.S. Sholl, Combining density functional theory and cluster expansion methods to predict H-2 permeance through Pd-based binary alloy membranes, Journal of Chemical Physics 128(14) (2008).

[19] M.P. Hyman, B.T. Loveless, J.W. Medlin, A density functional theory study of H2S decomposition on the (111) surfaces of model Pd-alloys, Surface Science 601(23) (2007) 5382-5393.

[20] C.G. Sonwane, J. Wilcox, Y.H. Ma, Achieving optimum hydrogen permeability in PdAg and PdAu alloys, Journal Of Chemical Physics 125(18) (2006).

[21] C.G. Sonwane, J. Wilcox, Y.H. Ma, Solubility of hydrogen in PdAg and PdAu binary alloys using density functional theory, Journal Of Physical Chemistry B 110(48) (2006) 24549-24558.

[22] D.R. Alfonso, A.V. Cugini, D.S. Sholl, Density functional theory studies of sulfur binding on Pd, Cu and Ag and their alloys, Surface Science 546(1) (2003) 12-26.

[23] O.M. Lovvik, R.A. Olsen, Density functional calculations on hydrogen in palladium-silver alloys, 2002. pp. 332-337.

[24] O.M. Lovvik, R.A. Olsen, Density functional calculations on hydrogen in palladium-silver alloys, 2002. pp. 332-337.

[25] G.W. Watson, R.P.K. Wells, D.J. Willock, G.J. Hutchings, A comparison of the adsorption and diffusion of hydrogen on the {111} surfaces of Ni, Pd, and Pt from density functional theory calculations, Journal of Physical Chemistry B 105(21) (2001) 4889-4894.

[26] G.W. Watson, R.P.K. Wells, D.J. Willock, G.J. Hutchings, Ab initio simulation of the interaction of hydrogen with the {111} surfaces of platinum, palladium and nickel. A possible explanation for their difference in hydrogenation activity, Chemical Communications(8) (2000) 705-706.

[27] V. Pallassana, M. Neurock, L.B. Hansen, B. Hammer, J.K. Norskov, Theoretical analysis of hydrogen chemisorption on Pd(111), Re(0001) and Pd-ML/Re(0001), Re- ML/Pd(111) pseudomorphic overlayers, Physical Review B 60(8) (1999) 6146-6154.

[28] E. Broclawik, Quantum chemical description of catalytic activation of the C-H bond, Polish Journal of Chemistry 72(7) (1998) 1551-1564.

[29] V. Ledentu, W. Dong, P. Sautet, Ab initio study of the dissociative adsorption of H-2 on the Pd(110) surface, Surface Science 413 (1998) 518-526.

[30] O.M. Lovvik, R.A. Olsen, Adsorption energies and ordered structures of hydrogen on Pd(111) from density-functional periodic calculations, Physical Review B 58(16) (1998) 10890-10898.

[31] W. Dong, V. Ledentu, P. Saute, G. Kresse, J. Hafner, A theoretical study of the H-induced reconstructions of the Pd(110)surface, Surface Science 377(1-3) (1997) 56-61.

[32] W. Dong, G. Kresse, J. Hafner, Dissociative adsorption of H-2 on the Pd(111) surface, Journal Of Molecular Catalysis A-Chemical 119(1-3) (1997) 69-76.

[33] W. Dong, J. Hafner, H-2 dissociative adsorption on Pd(111), Physical Review B 56(23) (1997) 15396-15403.

[34] R.A. Olsen, G.J. Kroes, O.M. Lovvik, E.J. Baerends, The influence of surface motion on the direct subsurface absorption of H-2 on Pd(111), Journal of chemical Physics 107(24) (1997) 10652-10661.

[35] N.M. Peachey, R.C. Snow, and R.C. Dye. “Composite Pd/Ta metal membranes for hydrogen separation.” Journal of Membrane Sciences 111 (1996): 123-133.

[36] A.G. Knapton. “Palladium alloys for hydrogen diffusion membranes.” *Platinum Metals Review* 21 (2) (1977): 44-50.

[37] T.B. Flanagan, W.A. Oates, The Palladium-Hydrogen System, Annual Review Of Materials Science 21 (1991) 269-304.

[38] A.C. Makrides, M.A. Newton, H. Wright and D.N. Jewett. “Separation of hydrogen by permeation.” U.S. Patent 3,350,846. 7 Nov. 1967.

[39] M.L. Doyle and I.R. Harris. “Palladium-rare earth alloys.” Platinum Metals Review 32 (1988): 130-140.

[40] A. Kulprathipanja, G.O. Alptekin, J.L. Falconer, J.D. Way, Effects of water gas shift gases on Pd-Cu alloy membrane surface morphology and separation properties, Industrial & Engineering Chemistry Research 43(15) (2004) 4188-4198.

[41] A. Kulprathipanja, G.O. Alptekin, J.L. Falconer, J.D. Way, Pd and Pd-Cu membranes: inhibition of H-2 permeation by H2S, 254(1-2) (2005) 49-62.

[42] A.L. Mejdell, H. Klette, A. Ramachandran, A. Borg, R. Bredesen, Hydrogen permeation of thin, free-standing Pd/Ag23% membranes before and after heat treatment in air, Journal of Membrane Science 307(1) (2008) 96-104.

[43] A. Unemoto, A. Kaimai, K. Sato, T. Otake, K. Yashiro, J. Mizusaki, T. Kawada, T. Tsuneki, Y. Shirasaki, I. Yasuda, Surface reaction of hydrogen on a palladium alloy membrane under co-existence of H2O, CO, CO2 or CH4, International Journal Of Hydrogen Energy 32(16) (2007) 4023-4029.

[44] J. Okazaki, D.A.P. Tanaka, M.A.L. Tanco, Y. Wakui, T. Ikeda, F. Mizukami, T.M. Suzuki, Preparation and hydrogen permeation properties of thin Pd-Au alloy membranes supported on porous alpha-alumina tube, Materials Transactions 49(3) (2008) 449-452.

[45] S.I. Pyun, W.J. Lee, T.H. Yang, Hydrogen diffusion through palladium-gold alloy coatings electrodeposited on palladium substrate under permeable boundary condition, Thin Solid Films 311(1-2) (1997) 183-189.

[46] D.L.McKinley and W. Nitro, U.S. Patent 3,247,648. 26 April 1966.

[47] S. Yuna, S. T. Oyamaa. Correlations in palladium membranes for hydrogen separation: A review. Journal of Membrane Science 375(1–2), (2011) 28–45.

[48] S. Uemiya, Y. Kude, K. Sugino, N. Sato, T. Matsuda, E. Kikuchi, A palladium/porous–glass composite membrane for hydrogen separation, Chem. Lett. (1988) 1687–1690.

[49] H. Masuda, K. Nishio, N. Baba, Preparation of microporous metal membrane using two-step replication of interconnected structure of porous glass, J. Mater. Sci. Lett. 13 (1994) 338–340.

[50] I.O. Mazali, A.G. Souza Filho, B.C. Viana, J. Mendes Filho, O.L. Alves, Sizecontrollable synthesis of nanosized-TiO2 anatase using porous Vycor glass as template, J. Nanopart. Res. 8 (2006) 141–148.

[51] S. Uemiya, N. Sato, H. Ando, Y. Kude, T. Matsuda, E. Kikuchi, Separation ofhydrogen through Pd thin film supported on a porous glass tube, J. Membr.Sci. 56 (1991) 303–313.

[52] A.J. Burggraaf, Important characteristics of inorganic membranes, in: A.J. Burggraaf, L. Cot (Eds.), Fundamentals of Inorganic Membrane Science and Technology, Elsevier, Amsterdam, 1996, pp. 22–28.

[53] S.N. Paglieri, J.D. Way, Innovations in palladium membrane research, Sep.Purif. Rev. 31 (2002) 1–169.

[54] S.T. Oyama, Y. Gu, Hydrogen-Selective Silica-Based Membrane, US Patent 7,179,325, Feb 20, 2007, Assigned to Virginia Tech Intellectual Properties Inc.

[55] D.R. Askeland, The Science and Engineering of Materials, 3rd ed., PWS Publishing Company, Boston, 1994.

[56] D.R. Lide (Ed.), CRC Handbook of Chemistry and Physics, 89th Edition, CRC Press, Boca Raton, Florida, 2008; Section 12, Properties of Solids; Thermal and Physical Properties of Pure Metals, 12–197.

[57] S.-E. Nam, K.-H. Lee, Hydrogen separation by Pd alloy composite membranes: introduction of diffusion barrier, J. Membr. Sci. 192 (2001) 177–185.

[58] I.P. Mardilovich, Y. She, Y.H. Ma,M.-H. Rei, Defect-free palladium membranes on porous stainless-steel support, AIChE J. 44 (1998) 310–322.

[59] S.K. Gade, P.M. Thoen, J.D. Way, Unsupported palladium alloy foil membranes fabricated by electroless plating, J. Membr. Sci. 316 (2008) 112–118.

[60] J. Shu, A. Adnot, B.P.A. Grandjean, S. Kaliaguine, Structurally stable composite Pd–Ag alloy membranes: introduction of a diffusion barrier, Thin Solid Films 286 (1996) 72–79.

[61] I.P. Mardilovich, E.S Ma##Y.H. Engwall, Dependence of hydrogen flux on the pore size and plating surface topology of asymmetric Pd-porous stainless steel membranes, Desalination 144 (2002) 85–89.

[62] S.-E. Nam, K.-H. Lee, A study on the Pd/nickel composite membrane by vacuum electrodeposition, J. Membr. Sci. 170 (2000) 163.

[63] R.W. Pierce, Method for Making a Fine Porosity Filter Element, US Patent 3,241,298, Mar 22, 1966.

[64] N. Jemaa, J. Shu, S. Kaliaguine, P.A. Grandjean, Thin palladium film formation on shot peening modified porous stainless steel substrates, Ind. Eng. Chem. Res. 35 (1996) 973–977.

[65] P. Quicker, V. Höllein, R. Dittmeyer, Catalytic dehydrogenation of hydrocarbons in palladium composite membrane reactors, Catal. Today 56 (2000) 21–34.

[66] S. Uemiya, Y. Kude, K. Sugino, N. Sato, T. Matsuda, E. Kikuchi, A palladium/porous–glass composite membrane for hydrogen separation, Chem. Lett. (1988) 1687–1690.

[67] H. Kikuchi, Medium for separating hydrogen, JP Patent 62-273,029, 1987, Assigned to ISE Chem Ind.

[68] M.E. Ayturk, Y.H. Ma, Electroless Pd and Ag deposition kinetics of the composite Pd and Pd/Ag membranes synthesized from agitated plating baths, J. Membr. Sci. 330 (2009) 233–245.

[69] G. Xomeritakis, Y. Lin, CVD synthesis and gas permeation properties of thin Pd/alumina membranes, AIChE J. 44 (1998) 174–183.

[70] O. Altinisik, M. Dogan, G. Dogu, Preparation and characterization of Pd-plated porous glass for hydrogen enrichment, Catal. Today 105 (2005) 641–646.

[71] R. Bhandari, Y.H. Ma, Pd–Ag membrane synthesis: the electroless and electroplating conditions and their effect on the deposits morphology, J. Membr. Sci. 334 (2009) 50–63.

[72] J. Ye, G. Dan, Q. Yuan, The preparation of ultrathin palladium membranes, Key Eng. Mater. 61 (1991) 437–442.

[73] N. Itoh, T. Akiha, T. Sato, Preparation of thin palladium composite membrane tube by a CVD technique and its hydrogen permselectivity, Catal. Today 104 (2005) 231–237.

[74] C.-S. Jun, K.-H. Lee, Palladium and palladium alloy composite membranes prepared by metal–organic chemical vapor deposition method (cold-wall), J. Membr. Sci. 176 (2000) 121–130.

[75] G. Xomeritakis, Y.S. Lin, Fabrication of a thin palladium membrane supported in a porous ceramic substrate by chemical vapor deposition, J. Membr. Sci. 120 (1996) 261–272.

[76] D.M. Mattox, Handbook of Physical Vapor Deposition (PVD) Process, Noyes Publications, Park Ridge, NJ, 1998.

[77] G. Xomeritakis, Y.S. Lin, Fabrication of thin metallic membranes by MOCVD and sputtering, J. Membr. Sci. 133 (1997) 217–230.

[78] Z. Hongbin, X. Guoxing, Preparation and characterization of Pd–Ag alloy composite membrane with magnetron sputtering, Sci. China, Ser. B: Chem. 42 (1999) 581–588.

[79] J. Shu, B.P.A. Grandjean, A.V. Neste, S. Kaliaguine, Catalytic Pd-based membrane reactors: a review, Can. J. Chem. Eng. 69 (1991) 1036–1060.

[80] H.P. Hsieh, Inorganic Membranes for Separation and Reaction, Elsevier Publishers, Amsterdam, 1996.

[81] S.-E. Nam, K.-H. Lee, A study on the Pd/nickel composite membrane by vacuum electrodeposition, J. Membr. Sci. 170 (2000) 163.

[82] B.H. Howard, R.P Killmeyer, K.S. Rothenberger, A.V. Cugini, B.D. Morreale, R.M. Enick and F. Bustamante. “Hydrogen permeance of palladium-copper alloy

membranes over a wide range of temperatures and pressures." Journal of Membrane Science 241 (2004): 207-218.

[83] R.E. Buxbaum and T.L. Marker. "Hydrogen Transport through non-porous membranes of palladium-coated niobium, tantalum, and vanadium." Journal of Membrane Sciences 85. (1993): 29-38.

[84] F. Gielens, R. Knibbeler, P. Duysinx, H. Tong, M. Vortsman and J. Keurentjes. "Influence of steam and carbon dioxide on the hydrogen flux through thin Pd/Ag and Pd membranes." Journal of Membrane Science 279 (2006): 176-185.

[85] C. Higman, M. van der Burgt, Gasification, Elsevier Science, 2003.

[86] W. Wang, X. Pan, X. Zhang, W. Yang and G. Xiong. "The effect of co-existing nitrogen on hydrogen permeation through thin Pd composite membranes." Separation and Purification Technology 54 (2007): 262-271.

[87] F. Gallucci, F. Chiaravalloti, S. Tosti, E. Drioli and A. Basile. "The effect of mixture gas on hydrogen permeation through a palladium membrane: experimental study and theoretical approach." International Journal of Hydrogen Energy 32 (2007): 1837-1845.

[88] F. Guazzone, E. Engwall and Y. Ma. "Effects of surface activity, defects and mass transfer on hydrogen permeance and n-value in composite palladium-porous stainless steel membranes." Catalysis Today 118 (2006): 24-31.

[89] J.E. Philpott. "Hydrogen diffusion technology: commercial applications of palladium membranes." Platinum Metals Review 29 (1) (1985): 12-16.

[90] R.T. James. Temperature and pressure effects on hydrogen permeation in palladium based membranes. Thesis. University of Maryland.

[91] C. van Rijn, M. Wekken, W. Nijdam and M. Elwenspoek. "Deflection and maximum load of microfiltration membrane sieves made with silicon micromachining." Journal of Microelectromechanical Systems 6.1 (1997): 48-54.

[92] H. Tong, J. Berenschot, M. De Boer, J. Gardeniers, H. Wensink, H. Jansen, W. Nijdam, M. Elwenspoek., F. Gielens and C. van Rijn. "Microfabrication of palladium-silver alloy membranes for hydrogen separation." Journal of Microelectromechanical Systems 12.5 (2003): 622-629.

[93] “Palladium Foil.” Goodfellow Corporation. Last accessed April 4, 2013, from https://www.goodfellowusa.com/catalog/.

[94] Agilent 3000 Micro Gas Chromatograph: User information. Agilent Technologies, Inc. 2850 Centerville Road Wilmington, DE 19808-1610 (2002):

[95] “General Service Pressure Gauge.” McMaster-Carr. Last accessed March 24, 2010, from http://www.mcmaster.com/#atmospheric-pressure-gauges/=6dh029.

[96] Omega Engineering, Inc. Last accessed March 24, 2010, from http://www.omega.com/.

[97] S.S. Zumdahl, Chemical Principles. Boston: Houghton Mifflin Harcourt Publishing Company. 2010. pp. 163-164.

[98] A. Li, W. Liang, R. Hughes, The effect of carbon monoxide and steam on the hydrogen permeability of a PD/stainless steel membrane. J Membrane Sci 2000; 165: 135-41.

[99] W.D. Davis, Diffusion of gases through metals . I . Diffusion of gases through palladium, US Atomic Energy Commission Report No. KAPL-1227, 1 October 1954.

[100] G. Toda, Rate of permeation and diffusion coefficient of hydrogen through palladium, J . Res . Inst . Catal . Hokkaido.

[101] G.L. Holleck, Diffusion and solubility of hydrogen in palladium and palladium-silver alloys, J. Phys. Chem. 74 (3) (1970) 503-511.

[102] R.C. Hurlbert, J.O. Konecny, Diffusion of hydrogen through palladium, J. Chem. Phys. 34 (2) (1961) 655-658.

[103] S.A. Koffler, J.B. Hudson, G.S. Ansell, Hydrogen permeation through alpha-palladium, Trans . Metall . Soc . AIME 245 (1969) 1735-1740.

[104] Y.A. Balovnev, Diffusion of hydrogen in palladium, Russ. J. Phys. Chem. 48 (3) (1974) 409-410.

[105] H. Katsuta, R.J. Farraro, R.B. McLellan, The diffusion of hydrogen in palladium, Acta Metall. 27 (1979) 1111-1114.

[106] Y. Huang and R. Dittmeyer. “Preparation of thin palladium membranes on a porous support with rough surface.” Journal of Membrane Science 302 (2007): 160-170.